X-linked immunodeficient mice with no functional Bruton's Tyrosine Kinase are protected from sepsis-induced multiple organ failure

Caroline E. O'Riordan*[1], Gareth S.D. Purvis[2], Debora Collotta[3], Bianka Wissua[4,5], Madeeha H. Sheikh[1], Gustavo Ferreira Alves[3], Nadine Krieg[4,5], Shireen Mohammad[1], Lauren A. Callender[1], Sina M. Coldewey[4,5], Massimo Collino[3], David R. Greaves[$2], and Christoph Thiemermann*[$1]

[1]William Harvey Research Institute, Queen Mary University of London, United Kingdom,
[2]Sir William Dunn School of Pathology, University of Oxford, Oxford,
[3]Department of Drug Science and Technology, University of Turin, Turin, Italy,
[4]Department of Anesthesiology and Intensive Care Medicine, Jena University Hospital, Jena, Germany,
[5]Septomics Research Center, Jena University Hospital, Jena, Germany.

[$] Donates shared senior authorship

* Correspondence:
Caroline Elizabeth O'Riordan
c.e.oriordan@qmul.ac.uk

Prof Christoph Thiemermann
c.thiemermann@qmul.ac.uk

Keywords: X-linked immunodeficient mice, Bruton's tyrosine kinase (BTK), sepsis, ibrutinib, cytokine storm, phagocytosis, NF-κB, NLRP3 inflammasome

Abstract

We previously reported the Bruton's tyrosine kinase (BTK) inhibitors ibrutinib and acalabrutinib improve outcomes in a mouse model of polymicrobial sepsis. Now we show that genetic deficiency of the BTK gene *alone* in *Xid* mice confers protection against cardiac, renal and liver injury in polymicrobial sepsis and reduces hyperimmune stimulation ('cytokine storm') induced by an overwhelming bacterial infection. Protection is due in part to enhanced bacterial phagocytosis *in vivo*, changes in lipid metabolism and decreased activation of NF-κB and the NLRP3 inflammasome. The inactivation of BTK leads to reduced innate immune cell recruitment and a phenotypic switch from M1 to M2 macrophages, aiding in the resolution of sepsis. We have also found that BTK expression in humans is increased in the blood of septic non-survivors, while lower expression is associated with survival from sepsis. Importantly no further reduction in organ damage, cytokine production or changes in plasma metabolites is seen in *Xid* mice treated with the BTK inhibitor ibrutinib, demonstrating that the protective effects of BTK inhibitors in polymicrobial sepsis are mediated solely by inhibition of BTK and not by off-target effects of this class of drugs.

Introduction

Sepsis is a common and life-threatening condition caused by a dysregulated host response to an infection, either bacterial, fungal or viral (1). Sepsis is a major public health problem leading to multiple organ dysfunction and death. Globally there are 50 million cases of sepsis resulting in the death of 11 million people every year representing 20% of all deaths worldwide (2). Despite intensive, supportive care and current treatments (antibiotic therapy and fluid resuscitation), no targeted therapies have proven effective at reducing mortality (3,4). There is

an urgent need for the development of pharmacological treatments for sepsis-induced organ dysfunction (5).

Bruton's tyrosine kinase (BTK) is well known as a critical component of the B-cell antigen receptor (BCR) signalling pathway (6). BTK is also involved in the activation of the toll-like receptor (TLR) signalling pathways (by binding to the TIR domain of TLR4 and TLR's adaptor molecules MyD88, and Mal) and the NLRP3 inflammasome (by binding to the ASC component) (7–9). Activation of both the TLR signalling pathway and the NLRP3 inflammasome play a pivotal role in the pathophysiology of sepsis (10,11). The expression of BTK is not restricted to B cells, as BTK is also expressed in cells of myeloid lineage, including macrophages and neutrophils (12,13), activation of which contributes to the pathophysiology of sepsis.

We have recently shown that the BTK inhibitors ibrutinib (first generation) and acalabrutinib (more selective, second generation) attenuate the systemic inflammation ('cytokine storm') and the multiple organ failure caused by sepsis in mice (14). Ibrutinib is already approved for the use in chronic lymphatic leukaemia, mantle cell lymphoma, Waldenstrom macroglobulinemia, and graft vs. host disease (15) and acalabrutinib in mantle cell lymphoma (16). The recent COVID-19 pandemic has driven the search for drugs that can be repurposed to either reduce virus load and/or the cytokine storm in patients with severe COVID-19 infections. It has been found that BTK activation and IL-6 production is increased in COVID-19 patients and the effects of acalabrutinib are currently being evaluated in these patients (17). Roschewski *et al*. showed that some severe COVID-19 patients receiving acalabrutinib had improved oxygenation and reduced CRP and plasma IL-6, suggesting that BTK inhibitors could be repurposed for diseases involving excessive inflammation.

Although we have proposed that the inhibition of BTK is the key driver of the observed beneficial effects of BTK inhibitors in sepsis, it is possible that some of the well-known off-target effects of these compounds account for or, at least, contribute to the beneficial effects observed (14). For instance, we identified that both ibrutinib and acalabrutinib strongly inhibit five different kinases: BTK, Bmx, ErbB4, RIPK2, and TEC. Our discovery that acalabrutinib and ibrutinib reduce inflammation and organ dysfunction in sepsis has triggered three important questions: (1) Does inhibition of BTK activity alone account for the observed beneficial effects? And (2) Does inhibition of systemic inflammation reduce the host response to infection and ultimately cause increased harm? (3) What effect does BTK inactivation have on the metabolomic profile of septic mice? Interest in metabolomic profiling is growing, as the metabolome is the result of expression and function of a multitude of proteins and, hence, has been suggested to be a sensitive readout of drug responses (18,19). The present study was designed to address these questions by inducing polymicrobial sepsis in mice with X-linked immunodeficiency (*Xid*). *Xid* mice have a missense mutation within the BTK gene (arginine to cysteine at position 28 (R28C)) in the N-terminally located pleckstrin homology domain, resulting in expression of a BTK protein that is functionally inactive (20,21). Having developed a model of sepsis in *Xid* mice (and wild-type mice, CBA background), we have investigated the impact of impaired BTK function on organ dysfunction, systemic inflammation (cytokine storm), changes in plasma metabolites, and bacterial clearance.

Methods

Ethical statement

The Animal Welfare Ethics Review Boards of Queen Mary University of London and The

Dunn School of Pathology in the University of Oxford approved all experiments in accordance with the Home Office guidance on the operation of Animals (Scientific Procedures Act 1986) published by Her Majesty's Stationery Office and the Guide for the Care and Use of Laboratory Animals of the National Research Council. Work was conducted under U.K. Home Office project licence number PCF29685 and P144E44F2.

Mice

This study was carried out on twenty-three 10-week-old, male CBA mice (Charles River Laboratories UK Ltd., Kent, UK) and twenty-one 10-week-old, male CBA/CaHN-*Btk*^{xid}/J (*Xid)* mice (from Jackson laboratory), weighing 25–30 g and kept under standard laboratory conditions. Six mice were housed together (in each cage) with access to a chow diet and water *ad libitum*. They were subjected to a 12-h light and dark cycle with a temperature maintained at 19–23°C. Group sizes for each experiment were calculated following power calculations based on previous studies (14).

Polymicrobial sepsis

Cecal ligation and puncture (CLP) was performed in 10-week-old male CBA (wild type) or *Xid* mice as previously described (14,22). Mice were randomly assigned to undergo CLP or sham-operated surgery, the surgeon was blinded to the genotype of the mouse. Briefly, mice were anesthetised with isoflurane (2% delivered in O_2) and the cecum was fully ligated below the ileocecal valve. A double puncture was made with a 18G needle into the cecum and a small amount of faeces was squeezed out after which the cecum was returned to its anatomical position, then the laparotomy was closed. All animals received fluids (5 ml/kg saline into abdomen before closure and 10 ml/kg saline s.c., immediately after surgery), antibiotics (Imipenem/Cilastatin; 20 mg/kg body weight s.c.), and analgesics (buprenorphine; 0.05 mg/kg body weight i.p.) at 6 h and 18 h after surgery. Sham-operated mice underwent the same procedure, but without CLP. At 1 h after CLP, WT or *Xid* mice received 30 mg/kg ibrutinib (Selleck Chemicals) intravenously.

A clinical score for monitoring the health of experimental mice was used to evaluate the symptoms consistent with murine sepsis. The maximum score of 6 comprised the presence of the following signs: lethargy, piloerection, tremors, periorbital exudates, respiratory distress, and diarrhoea. Mice with a clinical score >3 were defined as exhibiting severe sepsis, against a moderate sepsis for a score ≤3. Animals were culled at 24 h after the onset of sepsis (CLP).

Assessment of cardiac function *in vivo*

At 24 h post CLP, mice were anesthetised (0.5 - 2% isoflurane in O_2); body temperature was maintained at 37°C and heart rate was maintained at 450 bpm. Then, cardiac function was assessed by M-mode and B-mode echocardiography using the VisualSonics Vevo 3100 echocardiographic system and a MX550D transducer. The following parameters were measured: left ventricular ejection fraction, fractional shortening, fractional area change, cardiac output, stroke volume and myocardial performance index, as described previously (14).

Kidney dysfunction and hepatocellular injury

After 24 h, mice were sacrificed by terminal cardiac puncture, where terminal blood samples were immediately decanted into 1.3 ml serum gel tubes (Sarstedt, Nürnbrecht, Germany). Blood was allowed to coagulate for at least 10 min at room temperature, then samples were centrifuged at 9000 rpm for 3 min to separate the serum. Then 100 µl of serum was snap frozen in liquid nitrogen and sent to an independent veterinary testing laboratory (MRC Harwell Institute, Oxford, UK) to evaluate the following biomarkers in a blinded fashion: Urea and

creatinine (as markers of renal dysfunction), alanine aminotransferase (ALT), aspartate transaminase (AST) (markers of hepatocellular injury) and lactate dehydrogenase (LDH) (marker of cell injury).

Quantification of immune cells after peritoneal lavage

Peritoneal lavage exudate was collected by injecting 5 ml of 2 mM of EDTA in PBS into the peritoneal cavity. After gentle massaging, approximately 4ml of exudate was removed with an 18G needle**.** Cells were washed in FACS buffer (0.05 % BSA, 2 mM EDTA in PBS pH 7.4) and then blocked using anti-CD16/32 (Biolegend) for 10 min at 4°C. Peritoneal cells were analysed using anti-CD45 (clone 30-F11; BioLegend), anti-CD11b (clone M1/70; BioLegend), anti-F4/80 (clone BM8; BioLegend), anti-Ly6G (clone 1A8; BioLegend), anti-CD206 (clone C068C2; BioLegend), and anti-MHCII (clone. M5/114.15.2; BioLegend) antibodies. Absolute cell count was calculated by the addition of counting beads (BioLegend). Data were acquired using BD LSR II Fortessa (Becton Dickinson) and analysed using FlowJo analysis software (version 10.6, Treestar Inc.). The gating strategy is depicted in supplementary Figure S1.

Cytokine analysis

The principle of multiplex flow immunoassay technology has been reviewed previously (23,24). Cytokines, chemokines and a growth factor were determined in serum by Bio-Plex Pro Mouse Chemokine 31-Plex panel assay (Bio-Rad, Kabelsketal, Germany). The cytokines IL-1ß, –2, –4, –6, –10, –16, CCL1, –2, –3, –4, –5, –7, –11, –12, –17, –19, –20, –22, –24, –27, IFN-γ, TNF-α and the chemokines CX3CL1, CXCL1, –2, –5, –10, –11, –12 ,–13, –16 and the growth factor GM-CSF were measured according to the manufacturer's instructions.

Bacteria counting

Accurate evaluation of the number of bacteria in peritoneal lavage fluid and blood samples was performed by flow cytometry using the SYTO BC bacteria counting kit (Thermo Fischer Scientific).

Phagocytic ability

Peritoneal lavage exudate containing neutrophils and macrophages was obtained 24 h after CLP as described above. pHrodo™ red E.Coli bioparticles™ (Thermo Fischer Scientific) were resuspended in live cell imagining solution (BioLegend) at 10 mg/ml and 10 µL of bioparticles were opsonised with 20 µL of fresh serum for 1h at 37°C under gentle agitation, after which they were washed and resuspended in 10 µL of live cell imagining solution. 1×10^6 cells of peritoneal exudate were collected by centrifugation (300 g x 5 min) and resuspended in 890 µL of live cell imaging solution, after which 100 µl of fresh serum and 10 µL of optimised bioparticles were added and incubated for 45 min at 37°C under gentle agitation in the dark. Cells were washed and then blocked using anti-CD16/32 (Biolegend) for 10 min at 4°C followed by staining with surface markers anti-CD11b (clone M1/70; BioLegend), anti-Ly6G (clone 1A8; BioLegend) and anti-F4/80 (clone BM8; BioLegend) for 30 min at 4°C. 10,000 $CD11b^+$ cells were collected by Amnis® ImageStream®^{X} Mk II Imaging Flow Cytometer (Luminex) at a magnification of x40 and analysed by IDEAS software for each experimental sample. Neutrophils were identified as ($CD11b^+$, $Ly6G^+$, $F4/80^-$) and macrophages were identified as ($CD11b^+$, $Ly6G^-$, $F4/80^+$). This equated to approximately 7000 neutrophils and 2000 macrophages for both WT and *Xid* mice to undergo phagocytosis analysis via IDEAS software. For WT mice the average number of cells positive with pHrodo *E.coli* BioParticles

were 4200 neutrophils and 1,200 macrophages. For *Xid* mice the average number of cells positive with pHrodo *E.coli* BioParticles were neutrophils 5,600 and 1,200 macrophages.

Western blots

Immunoblot analyses of cardiac tissue samples were carried out using a semi-quantitative western blotting analysis. The antibody used were: 1:1,000 rabbit anti-Ser$^{176/180}$-IKKα/β, 1:1,000 rabbit anti-total IKKα/β, mouse anti-Ser$^{32/36}$-IκBα, mouse anti-total IκBα, rabbit anti-Tyr^{223}-BTK, rabbit anti-total BTK, rabbit anti-Tyr^{1217} PLCγ, rabbit anti-total PLCγ (from Cell Signaling), 1:5,000 rabbit anti NLRP3 inflammasome (from Abcam), mouse anti-caspase 1 (p20) (from Adipogen). The apex of the heart was taken and homogenized. Proteins were then extracted as previously described (25) and concentrations were quantified by bicinchoninic acid (BCA) protein assay (Thermo Fisher Scientific Rockford, IL). Proteins were separated by 8% sodium dodecyl sulfate (SDS)-PAGE and transferred to polyvinylidene fluoride membranes. Membranes were blocked in 10% milk solution with TBS-Tween and then incubated with the primary antibody overnight at 4°C. The next day the secondary antibody was added for 30 min at room temperature and visualized using the ECL detection system. Tubulin was used as loading control. The immunoreactive bands were analyzed by the Bio-Rad Image Lab Software™ 6.0.1 and results were normalised to the sham bands.

BTK gene expression in whole human blood

Original data was obtained from the gene expression omnibus under dataset number GDS4971 which was published by Parnell GP *et al*. (26). RNA isolated from whole-blood samples of survivors (n = 26) and non-survivors (n = 9) of sepsis as well as healthy participants (n = 18) over the course of 5 days was assayed on the Illumina HT-12 gene expression microarray consisting of 48,804 probes. The dataset was analysed for expression of BTK gene in these three groups. The figure was generated using R software (ver 4.0.2), gene expression is quantile normalization and log transformation of the data was applied. Significance was determined by a one-way ANOVA followed by a Bonferroni post hoc test.

Metabolomic analysis

Metabolites were analyzed by liquid chromatography coupled to triple quadrupole mass spectrometry (LC-MS/MS) using an ultra-high-performance liquid chromatography (UHPLC) system (Nexera LC-40 series) and the triple quadrupole mass spectrometer LCMS-8050, both from Shimadzu Deutschland GmbH (Duisburg, Germany). Samples were analyzed with a method for sphingosine-1-phosphate and sphingosine and the supplied method packages "primary metabolites", "phospholipids" and "lipid mediators" according to the manufacturer's protocols (Shimadzu Deutschland GmbH, Duisburg, Germany) with the following modifications: Twenty microliters of serum sample were precipitated by addition of 200 µL of methanol (LCMS-grade) in vials. Prior to processing, the methanol was spiked with internal standard (IS) solution in a final concentration of 45.45 nM. The supernatant was taken for analysis after 4 days of incubation at -80°C and subsequent centrifugation at 14,000 rcf for 10 min at 4 °C. Primary metabolites were analyzed using the HPLC Column Discovery® HS F5, 3 µm, 150 mm x 2.1 mm from Sigma-Aldrich Chemie GmbH (Munich, Germany). For phospholipids and lipid mediators, the 2.1 x 150 mm 2.6 µm particle size C8 Kinetex LC Column (Phenomenex Inc., Torrance, USA) was used. Sphingosine-1-phosphate and sphingosine were separated using a MultoHigh 100 RP 18-3µ 60 x 2 mm column (Chromatographie Service GmbH, Langerwehe, Germany) with intermittent runs for equilibration. Mass spectrometric detection was performed by multiple reactions monitoring

(MRM) after injection of 10 µl sample, unless stated otherwise. Further information on HPLC programs and solvents (Table S1), LCMS-8050 settings (Table S2), and recorded mass transitions of identified significantly changed analytes (Table S3-6) are listed in the Supplement. Metabolome primary data were analyzed and further processed with LabSolutions 5.91 and LabSolutions Insight 3.10 (Shimadzu Deutschland GmbH, Duisburg, Germany).

Statistics

Statistical differences were determined using a one-way ANOVA, followed by Bonferroni post hoc test or unpaired Student's t-test as appropriate (GraphPad Prism 8.0; significant when $P < 0.05$). Results are expressed as mean ± SEM of three independent experiments.

Metabolome data were determined by calculating area ratios for each analyte by dividing peak area of each analyte by peak area of the related IS. Data analysis for metabolome data was performed as follows: Readings below detection level were set to half of detection level for each analyte separately. Metabolome data was log2 transformed and normalized by subtracting median metabolite abundance per sample from all abundances of each sample. Normalization was carried out separately for primary metabolites, phospholipids and lipid mediators. Z scores were calculated using mean and standard deviation of all samples. Contrasts were analyzed pairwise between selected sample groups by unpaired t tests. P-values were Benjamini Hochberg adjusted (27) and log2 fold changes were reported (Supplementary Data). Analytes with adjusted P-values below 0.05 were considered significantly different. For a first exploratory overview a principal component analysis (PCA) was carried out using the normalised and scaled metabolome data. Data analysis was carried out using R version 3.4.4 (R Core Team 2018).

Results

***Xid* mice have 100% predicted survival rate**

When compared to sham-operated mice, WT mice subjected to cecal ligation and puncture (CLP) showed clinical signs of severe sepsis (80%; score >3). In contrast, all *Xid* mice subjected to CLP had a score of ≤3 indicating only moderate sepsis (Figure 1A). All mice in the WT-CLP group which received ibrutinib had a score of ≤3 indicating moderate sepsis and all mice in the *Xid*-CLP + ibrutinib group had a score ≤3. When compared to sham-operated mice, WT mice subjected to CLP experienced hypothermia (a rectal temperature of <30°C) at 24 h after the onset of CLP, whereas the rectal temperature of *Xid*-CLP, WT-CLP + ibrutinib and *Xid*-CLP + ibrutinib remained at 37°C (Figure 1B). A reduction in temperature to <30°C or a change of 5°C over time in each animal has been reported to predict death in mice with CLP (28). As mortality of animals is not an acceptable routine endpoint in the UK, we used the reduction in rectal temperature <30°C as a surrogate marker for mortality. Using this surrogate marker, we would predict the mortality of WT-CLP mice to be 90% (confirming that our model is a model of severe sepsis), while the predicted mortality of *Xid*-CLP mice would be 0% (e.g. 100% predicted survival; Figure 1C). WT mice receiving ibrutinib had a predicted mortality of 15%, whereas *Xid*-CLP mice receiving ibrutinib had a predicted mortality of 0%. When compared to sham-operated, WT mice subjected to CLP showed a decrease in heart rate, whereas the heart rate of *Xid*-CLP remained similar to that of sham-operated animals (Figure 1D). When compared to WT-CLP mice, the administration of ibrutinib 1 h after CLP attenuated the decline in heart rate in WT mice. Mice in the *Xid*-CLP + ibrutinib group had a similar heart rate to mice in the *Xid*-CLP group. *Xid*-CLP mice receiving ibrutinib had a higher heart rate than WT-CLP mice treated with ibrutinib.

Xid mice are protected from sepsis-induced cardiac dysfunction

Cardiac function was assessed *in vivo* by echocardiography. Figure 1E shows representative M-mode images in the short axis in sham-operated mice, CLP mice and CLP + ibrutinib mice of both genotypes. When compared to sham-operated, WT mice subjected to CLP showed a reduction in ejection fraction (EF), fractional shortening (FS), fractional area change (FAC), cardiac output (CO), stroke volume (SV) and an increase in myocardial performance index (MPI), indicating severe global, systolic cardiac dysfunction. In contrast, *Xid* mice subjected to CLP had only a very minor cardiac dysfunction and all indices of cardiac performance (EF, FS, FAC, CO, SV and MPI) were significantly improved from those measured in WT-CLP (Figure 1 F-K). Thus, the degree of cardiac dysfunction caused by CLP in *Xid* mice is significantly reduced when compared to that observed in WT-mice. When compared to WT-CLP mice (CBA background) treatment of WT-mice with ibrutinib 1 h after CLP attenuated the sepsis-induced cardiac dysfunction. In contrast, administration of ibrutinib to *Xid*-CLP mice had no effect on cardiac function (Figure1 F-K), indicating that the addition of ibrutinib in *Xid* mice with CLP results in no beneficial or deleterious effects due to off target actions of the drug.

Xid mice are protected from sepsis-induced kidney dysfunction and hepatocellular injury

Kidney dysfunction and hepatocellular injury was assessed by measuring serum creatinine, urea, ALT, AST and LDH. When compared to sham-operated mice, WT mice subjected to CLP had significant renal dysfunction (rise in urea and creatinine), hepatocellular injury (rise in ALT and AST) and cell injury (rise in LDH). In contrast, in *Xid* mice subjected to CLP, the degree of kidney dysfunction, hepatocellular injury and cell injury was significantly reduced when compared to WT-CLP mice (Figure 1 L-P). When compared to WT-CLP, treatment of WT-CLP mice with ibrutinib (1 h after CLP) significantly attenuated the rise of plasma/serum urea, creatinine, ALT, AST and LDH. In contrast, administration of ibrutinib in *Xid*-CLP mice had no significant effect on organ dysfunction (as this was prevented in *Xid*-mice). No significant difference was observed between WT-CLP + ibrutinib and *Xid*-CLP + ibrutinib for any of the parameters of organ dysfunction measured.

Xid mice do not present with systemic inflammation after polymicrobial sepsis

Using a multiplex array, we analysed 31 cytokines and chemokines in the serum of all animals. When compared to sham-operated mice, WT mice subjected to CLP sepsis showed a significant increase in the serum levels of pro-inflammatory cytokines TNF-α, IL-6 and IL-1β, the anti-inflammatory cytokine IL-10, neutrophils chemoattractant chemokines (KC & ENA-78), monocyte chemoattractant chemokines (MCP-1, MIP-1α and MIP-1β) and G-CSF. In contrast, the levels of these cytokines and chemokines in the serum of *Xid*-CLP were significantly reduced when compared to WT-CLP mice (Figure 2 A-J). When compared to WT-CLP, treatment of WT-CLP mice with ibrutinib (1 h after CLP) significantly attenuated the rise in cytokines and chemokines. In contrast, administration of ibrutinib in *Xid*-CLP-mice had no significant effect on the production of cytokines and chemokines (as this was prevented in *Xid*-mice). No significant difference was observed between WT-CLP + ibrutinib and *Xid*-CLP + ibrutinib for any cytokines and chemokines. The alterations of a further 21 cytokines and chemokines can be seen in Figure 2K and absolute values in supplementary Table 7.

Xid mice have fewer infiltrating immune cells in the peritoneum and enhanced polarisation to M2 macrophages in sepsis

We also evaluated the cell composition and phenotype in the peritoneal exudates of all animals by flow cytometry gating strategy seen in supplementary Figure 1. When compared to sham-

operated mice, WT mice subjected to CLP showed a significant increase in neutrophils and macrophages into the peritoneum. In contrast, *Xid*-CLP mice exhibited a significant reduction in the number of infiltrating neutrophils and macrophages when compared to WT-CLP mice (Figure 3A-C). Upon further analysis of the subsets of macrophages, we found that the macrophages obtained from WT-CLP mice are predominately of the pro-inflammatory M1 phenotype (60% M1 and 40% M2), while the macrophages of *Xid*-CLP are of the pro-resolving (anti-inflammatory) M2 phenotype (40% M1 and 60% M2) (Figure 3D-E).

Xid mice have fewer bacteria in peritoneum and blood due to increased phagocytosis in sepsis

In order to determine the mechanism that accounts for the improved outcome of BTK deficient mice, we investigated bacterial clearance *in vivo* in WT and *Xid*-mice at 24 h after the onset of CLP, as the survival of sepsis is dependent on the ability to clear bacteria. When compared to sham-operated mice, WT mice subjected to CLP exhibited elevated peritoneal and blood bacteria counts (Figure 4A-D). However, *Xid*-CLP mice had significantly fewer bacteria in the peritoneal cavity and blood than WT-CLP mice, showing that *Xid*-mice clear bacteria more efficiently than WT mice.

Clearance of bacteria is secondary to phagocytosis of bacteria in neutrophils and macrophages. *Xid* mice subjected to CLP presented with a reduced number of infiltrating immune cells, but also reduced bacterial counts at 24 h post CLP. This raises the question as to how fewer infiltrating immune cells are able to clear more bacteria? To address this question, we investigated whether *Xid* neutrophils and macrophages have increased phagocytic ability *in vivo*. We found that the percentage of neutrophils and macrophages, which are phagocytosing bacteria, are similar in WT-CLP and *Xid*-CLP mice. However, neutrophils and macrophages of *Xid*-CLP mice contain more bacteria per immune cell than WT-CLP mice, showing a 100% increase in phagocytic ability of both neutrophils and macrophages (Figure 4E-L). Collectively, this data clearly demonstrates that *Xid* mice with a deficiency in BTK show enhanced phagocytosis *in vivo* resulting in improved clearance of bacteria during a septic episode.

BTK, NF-κB and NLRP3 inflammasome are not activated in _Xid_ mice after polymicrobial sepsis

To understand the signalling mechanism associated with the observed cardiac dysfunction in CLP-sepsis, we investigated the effect of BTK deficiency in *Xid* mice on the activation of key signalling pathways of inflammation: BTK, NF-κB and NLRP3 inflammasome activation (Figure 5). When compared to sham-operated, WT mice subjected to CLP showed an increase of BTK activation as demonstrated by significant increases in the phosphorylation of cardiac BTK at Tyr^{223} and the phosphorylation of PLCγ at Tyr^{1217}. No activation of BTK was detected in *Xid* mice, even after CLP injury and the phosphorylation of cardiac BTK at Tyr^{223} and the phosphorylation of PLCγ at Tyr^{1217} in *Xid*-CLP mice were similar to that of sham-operated animals (Figure 5A-B).

NF-κB activation plays a key role in the pathophysiology of sepsis. When compared to sham-operated mice, WT-CLP mice exhibit a significant increase in NF-κB activation as demonstrated by significant increases in the phosphorylation of IKKα/β at $Ser^{176/180}$ and the phosphorylation of IκBα at $Ser^{32/36}$. When compared to WT-CLP mice, *Xid*-CLP mice the phosphorylation of IKKα/β at $Ser^{176/180}$ and IκBα at $Ser^{32/36}$ was significantly reduced, indicating

that the degree of activation of NF-κB caused by sepsis in the heart was significantly lower in *Xid*-mice than in WT-mice (Figure 5C-D).

When compared to sham-operated mice, WT mice subjected to CLP showed an increase in the activation of the NLRP3 inflammasome, demonstrated by an increase in the expression of the NLRP3 inflammasome and cleavage of pro-caspase-1 to caspase-1 in the heart (Figure 5E-F) as well as an increase the production of IL-1β in serum (Figure 2C). In contrast, *Xid*-CLP mice showed reduced activation of NLRP3 inflammasome as demonstrated by a decrease in the expression of the NLRP3 inflammasome, cleavage of pro-caspase-1 to caspase-1 (Figure 5E-F) and IL-1β when compared to WT-CLP mice (Figure 2C).

Xid mice show lower levels of sepsis-dysregulated metabolites

Using a targeted metabolomic approach, we detected 240 analytes in murine plasma. A two-dimensional principal component analysis (PCA) of all detected analytes (Figure 6), revealed a clear distinction between the two sham-operated mice groups (WT sham and *Xid* sham), the WT-CLP mice group and the three treated and/or *Xid* CLP-induced mice groups (*Xid* CLP, WT CLP + Ibrutinib and *Xid* CLP + Ibrutinib). The first principal component explained about 36 % of total variation among the six mice groups and separated the sham-operated mice from the CLP-induced mice groups. The second principal component explained about 13 % of total variation of all metabolites and achieved the same effect as PC2, but further it separated the CLP-induced WT mice group from the three mice groups *Xid* CLP, WT CLP + ibrutinib and *Xid* CLP + ibrutinib. Significant changes in analytes were identified and analyzed via hierarchical clustered z score heatmaps and their significant log2 fold changes of selected group comparisons were shown in log2 fold change heatmaps (Figure S2-S5). The heatmaps illustrate 55 significant primary metabolites (Figure S2), 138 significant phospholipids and their derivatives (Figure S3-S4) and 6 significant lipid mediators (Figure S5).

Figure 7 shows a sorting of 24 analytes that were significantly restored in the three mice groups *Xid*-CLP, WT-CLP + ibrutinib and *Xid*-CLP + ibrutinib to the initial levels of both sham-operated groups compared to the WT-CLP mice group. The ibrutinib treatment or the BTK inactivation or the combination of both restored 7 significant decreased and 17 significant increased analytes in CLP-induced WT-mice. The decreased analytes belonged predominantly to the lipid mediator's docosahexaenoic acid (DHA), eicosapentaenoic acid (EPA), lyso-platelet activating factor (lyso-PAF) and oleoylethanolamine (OEA). The bile acid taurodeoxycholic acid (TDCA), the phosphatidylinositol (PI) (34:2) and the primary metabolite niacinamide were also reduced. The increased analytes included 5 primary metabolites (dihydroxyphenylalanine (DOPA), creatine, carnosine, nicotinic acid, cytosine), 4 lysophosphatidylserines, 5 phosphatidylserines, 1 lysophosphatidylethanolamine, 1 lysophaphatidylglycerol and 1 phosphytidylethanolamine.

Sorting by analytes that were only significantly restored in *Xid*-CLP (Figure S6) showed 5 analytes. One analyte was increased, the primary metabolite kynurenine, and 4 analytes were decreased in the WT-CLP group and this included the primary metabolite uridine and one the phospholipids phosphatidylserine, phosphatidylethanolamine and phosphatidylinositol. Twenty-three analytes showed the sorting by significantly restored analytes in the mice groups *Xid* CLP and *Xid* CLP + Ibrutinib (Figure S7). The levels of 10 analytes (cGMP, creatinine, ursodeoxycholic acid (UDCA), deoxycholic acid (DCA), adenine, 1 lysophosphatidylserine, 1 lysophosphatidylglycerol, 3 lysophosphatidylethanolamines) were upregulated and 13 analytes (1 sphingomyelin, 6 phosphatidylcholines, 3 phosphatidylethanolamines,

2 phosphatidylserines, 1 phosphatidylinositol) were downregulated in CLP-induced wildtype mice. Analytes that were only restored in the mice group WT-CLP + ibrutinib could not be determined. The heatmap with analytes that were significantly restored in the mice groups WT-CLP + ibrutinib and *Xid*-CLP + ibrutinib (Figure S8) showed 1 increased primary metabolite (cholesterol) and 3 decreased phospholipids (2 phosphatidylserines and 1 lysophosphatidylserine). Detailed statistical information of the detectable analytes is shown in the Supplementary Data section.

Expression of BTK is increased in whole human blood of septic non-survivors

Parnell *et al*. collected whole blood of patients confirmed with sepsis (and healthy participants) over a 5-day time course with the first day of collection being within the initial 24 h of admission to the ICU (26). RNA was extracted from whole blood and gene expression was analysed by microarray. Three groups were collected, healthy participants, septic survivors and septic non-survivors. Dataset is available on the gene expression omnibus under GDS4791. We reanalysed this dataset for BTK expression in these three groups and found that at day 1 there is no significant differences in gene expression between healthy, septic survivors and septic non-survivors (Figure 8A&B). However, over the course of 5 days BTK expression increases in septic non-survivors and a significant difference between non-survivors and healthy participants as well as a significant difference between non-survivors and survivors is observed at day 5 (Figure 8C). There was no significant difference in BTK expression between septic survivors and healthy volunteers (Figure 8A-C).

Discussion

Sepsis is the overwhelming host response to infection (bacterial, fungal or viral) leading to shock and multiple organ dysfunction. We have previously reported that BTK inhibitors (ibrutinib, acalabrutinib) significantly attenuate sepsis-induced cardiac dysfunction and reduced inflammatory cytokine production, but BTK inhibitors have many off target effects (14). In the present study we investigated whether the beneficial effects are exclusively due to inhibition of BTK and how a reduction in systemic inflammation due to BTK loss of function mutation affects bacterial clearance *in vivo*. We addressed these questions by conducting a model of polymicrobial sepsis in *Xid* mice (which have a missense mutation in the BTK gene, resulting in BTK to be functionally impaired). We report here for the first time that *Xid* mice are protected from sepsis-induced multiple organ dysfunction (cardiac, renal and hepatocellular) due to increased bacterial clearance and suppression of systemic inflammation (cytokine storm) (please see Figure 9 for schematic diagram of the role of BTK in the pathophysiology of sepsis).

BTK inactivation prevents sepsis-induced multiple organ dysfunction

Sepsis results in multiple organ failure including cardiac dysfunction, renal dysfunction and hepatocellular injury. We report here for the first time that *Xid* mice subjected to sepsis are protected from developing cardiac dysfunction, hepatocellular injury and renal dysfunction. Most notably, ibrutinib significantly reduced sepsis-induced multiple organ failure in WT-mice but had no further beneficial effect in *Xid*-mice subjected to CLP-indicating that the observed beneficial effect of ibrutinib in WT-mice can solely be explained by inhibition of BTK-activity. We have previously reported that inhibition of BTK by ibrutinib or acalabrutinib attenuate sepsis-induced cardiac and renal dysfunction in C57Bl/6 mice (14) and additionally we have now shown that delayed administration of ibrutinib in WT-CLP (CBA background) also attenuates sepsis-induced cardiac dysfunction, renal dysfunction and hepatocellular injury, confirming that BTK inhibitors work in two different genetic backgrounds of mice. Furthermore, in this study we find that administration of ibrutinib (which inhibits a significant

number of kinases in addition to BTK, more than acalabrutinib) in *Xid*-CLP mice neither results in further beneficial effects nor any adverse effects on cardiac, renal or liver (dys)function. Inhibition of BTK reduces disease severity in animal models of sepsis-induced lung injury (29,30), warm liver ischemia and reperfusion (31) and spontaneous lupus nephritis (32). Thus, we here provide evidence that inhibition of BTK alone is sufficient to prevent sepsis-induced multiple organ injury.

BTK inactivation results in enhanced bacterial phagocytosis

We then investigated the mechanism(s) by which inactivation of BTK protects mice against sepsis-induced multiple organ failure. In septic patients, an essential treatment is early source control (removal of infection), which is associated with improved outcomes (33). We found that CLP in *Xid* mice results in a reduction of the number of bacteria in both peritoneum and blood (at 24 h after onset of CLP) when compared to WT-CLP mice. This may well be due to an increase in bacterial phagocytosis in *Xid* mice. Macrophages obtained from *Xid*-mice do not show defects in in phagocytosis (34,35) and we found that the percentage of phagocytosing cells are similar in both WT and *Xid* mice. We discovered, however, that macrophages obtained from *Xid*-mice with sepsis had taken up a significantly larger number of bacteria. This was also true for neutrophils from *Xid*-mice. We believe that the increase in phagocytosis by macrophages and neutrophils from *Xid*-mice *in vivo* could explain the observed increase in clearance of bacteria in peritoneum and blood. Beguem *et al*. found that monocytes from healthy volunteers stimulated with LPS and treated with evobrutinib resulted in an increased rate of phagocytosis *in vitro* due to a switch of macrophages from the pro-inflammatory M1 to the pro-resolving M2 phenotype and this was associated with reduced secretion of TNF-α (36). In addition, *Xid* mice infected with *F. tularensis* showed enhanced bacterial clearance from the lung and spleen, which correlated with a significant improvement of survival when compared to wild-type controls (37).

This raises the question of the underlying mechanisms that enables or drives increased phagocytosis in *Xid*-mice? Neither inhibition of BTK activity with ibrutinib nor inactivation of BTK in *Xid* mice affects monocyte FcγR-mediated phagocytosis, but it does supress FcγR-mediated cytokine production. The decrease of calcium flux due to BTK inhibition also does not affect phagocytosis, but does decrease cytokine production (34). BTK inhibition results in the polarisation to M2 macrophages (which have greater phagocytic ability (38)), demonstrated by increased expression of CD206. CD206 is involved in phagocytosis of a number of bacterial strains. For example, monocyte-derived macrophages that express high levels of CD206 phagocytosed 78% of *E.coli*, while monocyte-derived macrophages that express low levels of CD206 only phagocytosed 30% of *E.coli* (39). Excessive activation of neutrophils is known to decrease survival and enhance susceptibility to subsequent bacterial infections (40). One mechanism that may contribute to the pathology of sepsis is the release of neutrophil extracellular traps as they contain the beneficial antimicrobial nuclear proteins but also damaging citrullinated histones, elastase, myeloperoxidase and MMP-3 (41,42). The release of neutrophil extracellular traps results in ineffective phagocytosis (43). Florence *et al*. showed that BTK was increased in the lung neutrophils and inhibiting BTK protected mice against lethal influenza by reducing the release of neutrophil extracellular traps. The decrease of neutrophil extracellular traps was also observed in human peripheral blood neutrophils incubated with influenza and BTK inhibitor (30). However, the exact molecular mechanisms underlying this phenomenon are yet to be elucidated. Future studies are required to increase our understanding as to how *Xid* macrophages and neutrophils phagocytose more bacteria per immune cell.

BTK inactivation results in reduced infiltration of the peritoneum with innate immune cells

BTK plays a fundamental role in signalling and function of B cells, but BTK is also highly expressed in myeloid cells such as macrophages and neutrophils (9) and inactivation of BTK results in reduced cell-mediated inflammatory responses (44,45). We report here that *Xid*-CLP mice have reduced infiltrating innate immune cells (macrophages and neutrophils) in the peritoneum (site of infection). We propose that this may lead to a reduction of the formation of cytokines/chemokines in the serum and, hence, will prevent the cytokines storm.

BTK inactivation results in M2 polarisation

Macrophages play an important role in the two phases of sepsis (early pro-inflammatory phase and the later anti-inflammatory phase), as they can have either pro-inflammatory or anti-inflammatory properties. Initially, M1 macrophages (pro-inflammatory) activate inflammation by secreting TNF-α, IL-1β, IL-6 and IL-12 to promote the removal of the pathogen, then M2 macrophages repair tissue and resolve inflammation by secreting cytokines including IL-10 (46,47). If the M1 macrophage-driven pro-inflammatory response cannot be controlled, the resultant cytokine storm can be a key driver of the severity of sepsis leading to organ failure and death (48). From our experiments we conclude that a loss of function or inhibition of BTK drives the switch from the pro-inflammatory M1 phenotype to pro-resolving M2 phenotype in response to LPS (49). Here we report that macrophages obtained from septic *Xid*-mice have a pro-resolving M2 phenotype, whereas macrophages obtained from septic WT-mice have the M1 phenotype. Most notably, macrophages of the M2 phenotype have a greater phagocytotic function resulting in increased clearance of apoptotic cells and an acceleration of resolution (38). Indeed, M2 macrophages protect against sepsis-induced lung injury (50) and sepsis-induced acute kidney injury (51). Transplantation of M2 macrophages has been suggested as a potential therapeutic approach for sepsis-induced lung injury (50).

BTK inactivation reduces the activation of NF-κB

BTK plays a pivotal role in the activation of TLRs and, hence, the signalling steps leading to the activation of NF-κB (7), which plays a key role in the pathophysiology of septic cardiomyopathy (52). Here we report that *Xid* mice subjected to polymicrobial sepsis have a reduced activation of BTK and NF-κB (measured as phosphorylation of IKKα/β and IκBα) in the heart. We have previously reported that BTK inhibitors ibrutinib or acalabrutinib reduce the activation of cardiac BTK and NF-κB in mice subjected to sepsis (14). Furthermore, we have shown that inhibition of NF-κB activation with an inhibitor of IKK also attenuates the cardiac dysfunction associated with polymicrobial sepsis (52). Purvis *et al*. showed that ibrutinib treatment attenuated the activation of NF-κB and gene expression of cytokines in the diabetic kidney and liver (45). Thus, we propose that an impairment in the activation of BTK in *Xid* mice leads to reduced activation of NF-κB in the heart, which contributes to or accounts for the observed reduction in organ injury and dysfunction observed in *Xid*-mice with sepsis.

BTK inactivation prevents the cytokine storm

Activation of NF-κB leads to an increase in the production of cytokines and chemokines such as the pro-inflammatory cytokines TNF-α, IL-6, IL-1β and the anti-inflammatory cytokine IL-10, neutrophils chemoattractant chemokines (KC & ENA-78), monocyte chemoattractant chemokines (MCP-1, MIP-1α and MIP-1β) and G-CSF, all of which contribute to the systemic inflammation and organ dysfunction associated with sepsis (53). Out of all these cytokines, the ones increased most in our model of murine sepsis were IL-6, KC and MCP-1. The levels of IL-8 and monocyte chemoattractant protein-1 (MCP-1) are associated with early 48-hr and 28-

day mortality in sepsis patients (54). Most notably, we report that in *Xid*-mice subjected to CLP-sepsis, all of these cytokines and chemokines are markedly reduced. WT-CLP mice treated with ibrutinib also show reduced production of sepsis-associated cytokines and chemokines and no difference is observed with the addition of ibrutinib to *Xid*-CLP mice. Thus, an impairment of BTK activation in *Xid*-mice prevents NF-κB and NLRP3-dependent, systemic inflammation (cytokine storm) resulting in a reduction in organ injury/dysfunction.

BTK inactivation reduces the activation of the NLRP3 inflammasome

BTK is also involved in the assembly/activation of the NLRP3 inflammasome in both mice and humans (8,55). The activation of the NLRP3 inflammasome also plays a role in the pathophysiology of sepsis and septic cardiomyopathy (56). Pharmacological inhibition of NLRP3 activation with MCC950 (NLRP3 inflammasome inhibitor) reduced the neurological and cognitive impairment in septic animals (57). It has also been reported that genetic deficiency of NLRP3 promotes resolution of inflammation in polymicrobial sepsis (58). We report here that the activation of the NLRP3 inflammasome (measured as NLRP3 activation, caspase-1 activation and IL-1β release) was largely reduced in *Xid*-mice subjected to CLP when compared to WT-mice with sepsis. We previously reported that BTK inhibitors (ibrutinib or acalabrutinib) inhibit the activation of the NLRP3 inflammasome and production of IL-1β in septic animals (14). Purvis *et al*. showed that ibrutinib treatment also attenuated the activation NLRP3 inflammasome in the diabetic kidney and liver (45). Thus, we propose that prevention of the activation of the NLRP3 inflammasome secondary to reduced activation of BTK importantly contributes to the reduction in inflammation and organ dysfunction observed in septic *Xid*-mice.

BTK inactivation restores dysregulated metabolites

PCA showed that 49% of the total variance of all metabolites formed three well separable clusters. The metabolomic profiles of CLP-induced WT mice formed one cluster and was clearly distinguishable from a second cluster (WT sham-operated and *Xid* sham-operated) and a third cluster consisting of the three groups *Xid*-CLP, WT-CLP + ibrutinib and *Xid*-CLP + ibrutinib. The common clustering of the latter three groups supports the assumption that the inhibition of BTK alone is responsible for the partial restoration of dysregulated metabolites in sepsis.

Host defense toward bacterial infection is a complex interplay of several mechanisms including inflammation, coagulation, immune activation, hypoxia and metabolic reprogramming. Specifically, the regulation and impact of the metabolic changes is known to play an important role in the pathophysiology of sepsis (59). We demonstrated in this study that deregulated members of lipid mediators, phospholipids, primary metabolites and bile acids in CLP-induced WT-mice were restored by ibrutinib (in WT-mice) and/or by inactivation of the BTK gene (*Xid*-mice). The elevated and reduced plasma levels of some restored metabolites in the WT CLP group were already shown. For example, an increased metabolism of the lipid mediators AA and EPA could be found in plasma of sepsis patients (60). In addition, two other lipid mediators, OEA and lyso-PAF, were decreased in CLP-induced WT mice. Platelet-activating factor (PAF) is a proinflammatory mediator in systemic inflammation and its known to be upregulated in sepsis (61). Degradation of the immediate precursor lyso-PAF is probably a result of its increased transformation to PAF (62). The decreased levels of the lipid-amide OEA are probably a compensatory mechanism in sepsis-related weight loss and disturbed energy balance, because OEA is a modulator in food consumption and weight management and actually leads to satiation or meal termination (63). Even the restoration of the reduced bile acid TDCA and the elevated amino acid DOPA seems to be a positive regulatory mechanism.

TDCA ameliorates systemic inflammation, normalizes blood pressure, prevents kidney injury and prolongs survival in a mouse sepsis model (64). DOPA has anti-neuro inflammation effects and improved neuroplasticity in septic mice (65). The plasma of the WT-CLP group showed also increased levels of isoforms of the phospholipids species lysophaphatidylserine and PS, probably due to their procoagulant activity in sepsis (66,67). Some primary metabolites were also enhanced in septic mice and restored by ibrutinib administration and BTK inactivation such as the dysregulated precursors (cytosine, niacinamide, nicotinic acid) of nucleotide or nicotinate and nicotinamide metabolism (68,69). The restoration also included the loss of carnosine to plasma due to skeletal muscle wasting in sepsis (70) and the elevated levels of creatine presumably because of the known higher activity of creatine kinase to catalyze the urgently required ATP in developing sepsis (71). This data of restored metabolites demonstrates that *Xid* mice with a deficiency in BTK have a similar metabolomic profile in sepsis than WT-CLP-mice treated with ibrutinib.

In addition, the data in figures S5 and S6 reveal that *Xid* mice restored metabolites 7 times more than ibrutinib-treated mice (Fig. S7). Many of the additionally restored metabolites in *Xid* mice are known to be deregulated in sepsis such as adenine (72) creatinine (73) and kynurenine (74). An explanation for the different magnitude of restored metabolites in *Xid* mice in comparison with ibrutinib-treated mice could be the different number of inhibited kinases. Thus, the *Xid* mice seem to benefit from the inhibition of only one kinase, namely BTK, which in addition to reducing cytokine storm restores the sepsis-related dysregulation of specific metabolites.

BTK expression is increased in whole human blood of septic non-survivors

Currently the expression and/or activation of BTK in septic patients has not been reported. There are datasets available on the GEO and we reanalysed microarray data (GDS4971) of the time course of gene expression in healthy, septic survivors and septic non-survivors published by Parnell *et al*. (26). Interestingly, our analysis revealed an increase in expression of BTK in septic non-survivors, whereas BTK expression in septic survivors does not increase and is not different from healthy volunteers. Thus, increases in BTK expression in septic patients correlate with mortality, while lower levels of BTK expression are associated with survival from sepsis. There were no clear differences between cytokine expression of TNF-α, IL-6, MCP-1, CXCL1 in the three groups, expression of BTK was a better predictor of mortality rather than with the expression of any one cytokine. We have previously shown in septic mouse hearts that activation of BTK correlates with cardiac dysfunction (14). BTK activation also increases in whole blood of COVID-19 patients which, like septic patients, also present with excessive systemic inflammation (cytokine storm) (17).

Limitations of the Study

We have shown that *Xid*-mice subjected to CLP have increased bacterial clearance and reduced systemic inflammation (secondary to reduced activation of the NLRP3 inflammasome and NF-κB) and cardiac (organ) dysfunction. There is good evidence that mortality of patients with sepsis increases with an increase in the number of organs failing (SOFA scores). In the UK survival studies in septic models are not routinely conducted due to ethical reasons. Thus, we were unable to investigate the survival of *Xid* mice undergoing sepsis. It has been reported that a reduction in temperature <30°C or a change of temperature of 5°C over time predicts mortality in animals with sepsis (28). Using this more humane surrogate marker, we found that *Xid* mice

with sepsis have a predicted mortality of 0% (100% survival), while WT-mice with sepsis would have a predicted mortality of 90% (10% survival). We found that ibrutinib does not affect predicted mortality in *Xid*-CLP resulting in a predicted mortality of 0% (100% survival) and that delayed administration of ibrutinib in WT-CLP mice led to a predicated mortality of 15% (85% survival). It would be useful to confirm the impact of an impairment in BTK function in *Xid*-mice on outcome (mortality) in a more long-term sepsis model.

Conclusion

We report here for the first time that genetic inactivation of BTK is responsible for conferring protection against multiple organ failure in a clinically relevant model of sepsis. Most importantly we have shown that the inactivation of BTK in *Xid* mice results in an increase of bacterial phagocytosis in macrophages and neutrophils, thus, increasing bacterial clearance in both peritoneum and blood. Inactivation of BTK also results in a phenotypic switch of macrophages from M1 to the M2 phenotype, which aids in the resolution of sepsis. The suppression of the immune system by inactivated BTK leads to reduced activation of NF-κB and the NLRP3 inflammasome, therefore, preventing the induction of the cytokine storm. Metabolomic analysis revealed a dysregulation of metabolites in WT septic mice. Most notably, we found that inactivation of BTK in *Xid*-mice or administration of ibrutinib in WT mice is responsible for the (partial) restoration of dysregulated metabolites in sepsis. As the administration of ibrutinib to *Xid*-CLP mice did not result in any additional (beneficial) effects on the alterations in organ dysfunction, cytokine/chemokines formation and changes in metabolites caused by sepsis, our data strongly suggest that BTK inactivation is responsible for the observed effects of ibrutinib. Lastly, we have found that BTK expression in humans is increased in the blood of septic non-survivors, while lower expression is associated with survival from sepsis. Taken together our work suggests that BTK inhibitors maybe repurposed for the use in sepsis (or other conditions associated with excessive local or systemic inflammation including COVID-19) due to their ability to reduce systemic inflammation (cytokine storm), their ability to enhance the phagocytosis of macrophages and switch macrophages from the pro-inflammatory M1 to the anti-inflammatory M2 phenotype.

Acknowledgments

We would like to thank Hira Bahadur Ale for their technical assistance on the Amnis® ImageStream®^{X} Mk II Imaging Flow Cytometer. We thank Dominik Driesch (BioControl Jena GmbH, Jena, Germany) for statistical advice with respect to metabolome analysis.

C.E.O was sponsored by Barts and The London School of Medicine and Dentistry, Queen Mary University of London. This work was, in part, supported by William Harvey Research Limited and the William Harvey Research Foundation, the British Heart Foundation (Award number: RG/15/10/23915 to D.R.G), the Oxford BHF Centre of Research Excellence (Award number: RE/13/1/30181 to G.S.D.P and D.R.G.), the Federal Ministry of Education and Research (BMBF), Germany (Award number: 03Z22JN12 to S.M.C., Research Group Translational Septomics, Centre for Innovation Competence (ZIK) Septomics).

Authorship contributions

C.E.O., G.S.D.P., S.M.C., M.C., D.R.G. and C.T. conceived and designed the experiments. C.E.O., G.S.D.P., D.C., B.W., M.S., S.M., L.C., N.F. and G.A. performed the experiments. C.E.O., G.S.D.P., M.C., S.M.C., N.F., B.W., D.R.G., and C.T. analysed the data. C.E.O.

D.R.G. and C.T. contributed to the writing of the manuscript. All authors reviewed the manuscript before submission.

Conflict of Interest.

The authors declare that the research was conducted in the absence of any commercial or financial relationships that could be construed as a potential conflict of interest.

References

1. Singer M, Deutschman CS, Seymour CW, Shankar-Hari M, Annane D, Bauer M, Bellomo R, Bernard GR, Chiche J-DD, Coopersmith CM, et al. The Third International Consensus Definitions for Sepsis and Septic Shock (Sepsis-3). *JAMA* (2016) **315**:801–810. doi:10.1001/jama.2016.0287
2. Rudd KE, Johnson SC, Agesa KM, Shackelford KA, Tsoi D, Kievlan DR, Colombara D V, Ikuta KS, Kissoon N, Finfer S, et al. Global, regional, and national sepsis incidence and mortality, 1990-2017: analysis for the Global Burden of Disease Study. *Lancet (London, England)* (2020) **395**:200–211. doi:10.1016/S0140-6736(19)32989-7
3. Marshall JC. Why have clinical trials in sepsis failed? *Trends Mol Med* (2014) **20**:195–203. doi:10.1016/j.molmed.2014.01.007
4. Cavaillon J, Singer M, Skirecki T. Sepsis therapies: learning from 30 years of failure of translational research to propose new leads. *EMBO Mol Med* (2020) **12**: doi:10.15252/emmm.201810128
5. Martin L, Derwall M, Al Zoubi S, Zechendorf E, Reuter DA, Thiemermann C, Schuerholz T. The Septic Heart: Current Understanding of Molecular Mechanisms and Clinical Implications. *Chest* (2019) **155**:427–437. doi:10.1016/J.CHEST.2018.08.1037
6. Tsukada S, Saffran DC, Rawlings DJ, Parolini O, Allen RC, Klisak I, Sparkes RS, Kubagawa H, Mohandas T, Quan S. Deficient expression of a B cell cytoplasmic tyrosine kinase in human X-linked agammaglobulinemia. *Cell* (1993) **72**:279–90.
7. Jefferies CA, Doyle S, Brunner C, Dunne A, Brint E, Wietek C, Walch E, Wirth T, O'Neill LAJ. Bruton's tyrosine kinase is a Toll/interleukin-1 receptor domain-binding protein that participates in nuclear factor kappaB activation by Toll-like receptor 4. *J Biol Chem* (2003) **278**:26258–64. doi:10.1074/jbc.M301484200
8. Ito M, Shichita T, Okada M, Komine R, Noguchi Y, Yoshimura A, Morita R. Bruton's tyrosine kinase is essential for NLRP3 inflammasome activation and contributes to ischaemic brain injury. *Nat Commun* (2015) **6**:7360. doi:10.1038/ncomms8360
9. Weber ANR, Bittner Z, Liu X, Dang T-M, Radsak MP, Brunner C. Bruton's Tyrosine Kinase: An Emerging Key Player in Innate Immunity. *Front Immunol* (2017) **8**:1454. doi:10.3389/fimmu.2017.01454
10. Danielski LG, Giustina A Della, Bonfante S, Barichello T, Petronilho F. The NLRP3 Inflammasome and Its Role in Sepsis Development. *Inflammation* (2020) **43**:24–31. doi:10.1007/s10753-019-01124-9
11. Deng M, Scott MJ, Loughran P, Gibson G, Sodhi C, Watkins S, Hackam D, Billiar TR. Lipopolysaccharide clearance, bacterial clearance, and systemic inflammatory responses are regulated by cell type-specific functions of TLR4 during sepsis. *J Immunol* (2013) **190**:5152–60. doi:10.4049/jimmunol.1300496
12. Brunner C, Müller B, Wirth T. Bruton's Tyrosine Kinase is involved in innate and adaptive immunity. *Histol Histopathol* (2005) **20**:945–55. doi:10.14670/HH-20.945
13. Pal Singh S, Dammeijer F, Hendriks RW. Role of Bruton's tyrosine kinase in B cells and malignancies. *Mol Cancer* (2018) **17**:57. doi:10.1186/s12943-018-0779-z
14. O'Riordan CE, Purvis GSD, Collotta D, Chiazza F, Wissuwa B, Al Zoubi S, Stiehler

L, Martin L, Coldewey SM, Collino M, et al. Bruton's Tyrosine Kinase Inhibition Attenuates the Cardiac Dysfunction Caused by Cecal Ligation and Puncture in Mice. *Front Immunol* (2019) **10**:2129. doi:10.3389/fimmu.2019.02129

15. Sanford DS, Wierda WG, Burger JA, Keating MJ, O'Brien SM. Three Newly Approved Drugs for Chronic Lymphocytic Leukemia: Incorporating Ibrutinib, Idelalisib, and Obinutuzumab into Clinical Practice. *Clin Lymphoma Myeloma Leuk* (2015) **15**:385–391. doi:10.1016/j.clml.2015.02.019
16. Markham A, Dhillon S. Acalabrutinib: First Global Approval. *Drugs* (2018) **78**:139–145. doi:10.1007/s40265-017-0852-8
17. Roschewski M, Lionakis MS, Sharman JP, Roswarski J, Goy A, Monticelli MA, Roshon M, Wrzesinski SH, Desai J V, Zarakas MA, et al. Inhibition of Bruton tyrosine kinase in patients with severe COVID-19. *Sci Immunol* (2020) **5**: doi:10.1126/sciimmunol.abd0110
18. Cambiaghi A, Pinto BB, Brunelli L, Falcetta F, Aletti F, Bendjelid K, Pastorelli R, Ferrario M. Characterization of a metabolomic profile associated with responsiveness to therapy in the acute phase of septic shock. *Sci Rep* (2017) **7**:9748. doi:10.1038/s41598-017-09619-x
19. Leite HP, de Lima LFP. Metabolic resuscitation in sepsis: a necessary step beyond the hemodynamic? *J Thorac Dis* (2016) **8**:E552-7. doi:10.21037/jtd.2016.05.37
20. Rawlings DJ, Saffran DC, Tsukada S, Largaespada DA, Grimaldi JC, Cohen L, Mohr RN, Bazan JF, Howard M, Copeland NG. Mutation of unique region of Bruton's tyrosine kinase in immunodeficient XID mice. *Science* (1993) **261**:358–61. doi:10.1126/science.8332901
21. Thomas J, Sideras P, Smith C, Vorechovsky I, Chapman V, Paul W. Colocalization of X-linked agammaglobulinemia and X-linked immunodeficiency genes. *Science (80-)* (1993) **261**:355–358. doi:10.1126/SCIENCE.8332900
22. Zechendorf E, O'Riordan CE, Stiehler L, Wischmeyer N, Chiazza F, Collotta D, Denecke B, Ernst S, Müller-Newen G, Coldewey SM, et al. Ribonuclease 1 attenuates septic cardiomyopathy and cardiac apoptosis in a murine model of polymicrobial sepsis. *JCI insight* (2020) **5**: doi:10.1172/jci.insight.131571
23. Morgan E, Varro R, Sepulveda H, Ember JA, Apgar J, Wilson J, Lowe L, Chen R, Shivraj L, Agadir A, et al. Cytometric bead array: a multiplexed assay platform with applications in various areas of biology. *Clin Immunol* (2004) **110**:252–266. doi:10.1016/j.clim.2003.11.017
24. Varro R, Chen R, Sepulveda H, Apgar J. "Bead-Based Multianalyte Flow Immunoassays," in *Methods in molecular biology (Clifton, N.J.)*, 125–152. doi:10.1007/978-1-59745-323-3_9
25. Collino M, Pini A, Mugelli N, Mastroianni R, Bani D, Fantozzi R, Papucci L, Fazi M, Masini E. Beneficial effect of prolonged heme oxygenase 1 activation in a rat model of chronic heart failure. *Dis Model Mech* (2013) **6**:1012–20. doi:10.1242/dmm.011528
26. Parnell GP, Tang BM, Nalos M, Armstrong NJ, Huang SJ, Booth DR, McLean AS. Identifying Key Regulatory Genes in the Whole Blood of Septic Patients to Monitor Underlying Immune Dysfunctions. *Shock* (2013) **40**:166–174. doi:10.1097/SHK.0b013e31829ee604
27. Benjamini Y, Hochberg Y. Controlling the False Discovery Rate: A Practical and Powerful Approach to Multiple Testing. *J R Stat Soc Ser B* (1995) **57**:289–300. doi:10.2307/2346101
28. Mai SHC, Sharma N, Kwong AC, Dwivedi DJ, Khan M, Grin PM, Fox-Robichaud AE, Liaw PC. Body temperature and mouse scoring systems as surrogate markers of death in cecal ligation and puncture sepsis. *Intensive Care Med Exp* (2018) **6**:20.

doi:10.1186/s40635-018-0184-3
29. Zhou P, Ma B, Xu S, Zhang S, Tang H, Zhu S, Xiao S, Ben D, Xia Z. Knockdown of Burton's tyrosine kinase confers potent protection against sepsis-induced acute lung injury. *Cell Biochem Biophys* (2014) **70**:1265–1275. doi:10.1007/s12013-014-0050-1
30. Florence JM, Krupa A, Booshehri LM, Davis SA, Matthay MA, Kurdowska AK. Inhibiting Bruton's tyrosine kinase rescues mice from lethal influenza-induced acute lung injury. *Am J Physiol - Lung Cell Mol Physiol* (2018) **315**:L52. doi:10.1152/AJPLUNG.00047.2018
31. Palumbo T, Nakamura K, Lassman C, Kidani Y, Bensinger SJ, Busuttil R, Kupiec-Weglinski J, Zarrinpar A. Bruton Tyrosine Kinase Inhibition Attenuates Liver Damage in a Mouse Warm Ischemia and Reperfusion Model. *Transplantation* (2017) **101**:322–331. doi:10.1097/TP.0000000000001552
32. Chalmers SA, Glynn E, Garcia SJ, Panzenbeck M, Pelletier J, Dimock J, Seccareccia E, Bosanac T, Khalil S, Harcken C, et al. BTK inhibition ameliorates kidney disease in spontaneous lupus nephritis. *Clin Immunol* (2018) **197**:205–218. doi:10.1016/J.CLIM.2018.10.008
33. Rhodes A, Evans LE, Alhazzani W, Levy MM, Antonelli M, Ferrer R, Kumar A, Sevransky JE, Sprung CL, Nunnally ME, et al. Surviving Sepsis Campaign: International Guidelines for Management of Sepsis and Septic Shock: 2016. *Intensive Care Med* (2017) **43**:304–377. doi:10.1007/s00134-017-4683-6
34. Ren L, Campbell A, Fang H, Gautam S, Elavazhagan S, Fatehchand K, Mehta P, Stiff A, Reader BF, Mo X, et al. Analysis of the Effects of the Bruton's tyrosine kinase (Btk) Inhibitor Ibrutinib on Monocyte Fcγ Receptor (FcγR) Function. *J Biol Chem* (2016) **291**:3043–52. doi:10.1074/jbc.M115.687251
35. Mangla A, Khare A, Vineeth V, Panday NN, Mukhopadhyay A, Ravindran B, Bal V, George A, Rath S. Pleiotropic consequences of Bruton tyrosine kinase deficiency in myeloid lineages lead to poor inflammatory responses. *Blood* (2004) **104**:1191–1197. doi:10.1182/blood-2004-01-0207
36. Yasemin Beguem Alankus, Roland Grenningloh, Philipp Haselmayer AB and JB. Inhibition of Bruton's Tyrosine Kinase (BTK) Prevents Inflammatory Macrophage Differentiation: A Potential Role in RA and SLE - ACR Meeting Abstracts. in *American College of Rheumatology*, 70 (suppl 10).
37. Crane DD, Griffin AJ, Wehrly TD, Bosio CM. B1a cells enhance susceptibility to infection with virulent Francisella tularensis via modulation of NK/NKT cell responses. *J Immunol* (2013) **190**:2756–66. doi:10.4049/jimmunol.1202697
38. Rőszer T. Understanding the Mysterious M2 Macrophage through Activation Markers and Effector Mechanisms. *Mediators Inflamm* (2015) **2015**:1–16. doi:10.1155/2015/816460
39. Schulz D, Severin Y, Zanotelli VRT, Bodenmiller B. In-Depth Characterization of Monocyte-Derived Macrophages using a Mass Cytometry-Based Phagocytosis Assay. *Sci Rep* (2019) **9**:1925. doi:10.1038/s41598-018-38127-9
40. Liu F-C, Chuang Y-H, Tsai Y-F, Yu H-P. Role of Neutrophil Extracellular Traps Following Injury. *Shock* (2014) **41**:491–498. doi:10.1097/SHK.0000000000000146
41. Czaikoski PG, Mota JMSC, Nascimento DC, Sônego F, Castanheira FV e S, Melo PH, Scortegagna GT, Silva RL, Barroso-Sousa R, Souto FO, et al. Neutrophil Extracellular Traps Induce Organ Damage during Experimental and Clinical Sepsis. *PLoS One* (2016) **11**:e0148142. doi:10.1371/journal.pone.0148142
42. Colón DF, Wanderley CW, Franchin M, Silva CM, Hiroki CH, Castanheira FVS, Donate PB, Lopes AH, Volpon LC, Kavaguti SK, et al. Neutrophil extracellular traps (NETs) exacerbate severity of infant sepsis. *Crit Care* (2019) **23**:113.

doi:10.1186/s13054-019-2407-8
43. Manfredi AA, Ramirez GA, Rovere-Querini P, Maugeri N. The Neutrophil's Choice: Phagocytose vs Make Neutrophil Extracellular Traps. *Front Immunol* (2018) **9**:288. doi:10.3389/fimmu.2018.00288
44. de Porto AP, Liu Z, de Beer R, Florquin S, de Boer OJ, Hendriks RW, van der Poll T, de Vos AF. Btk inhibitor ibrutinib reduces inflammatory myeloid cell responses in the lung during murine pneumococcal pneumonia. *Mol Med* (2019) **25**:3. doi:10.1186/s10020-018-0069-7
45. Purvis GSD, Collino M, Aranda-Tavio H, Chiazza F, O'Riordan CE, Zeboudj L, Mohammad S, Collotta D, Verta R, Guisot NES, et al. Inhibition of Bruton's tyrosine kinase regulates macrophage NF-κB and NLRP3 inflammasome activation in metabolic inflammation. *Br J Pharmacol* (2020)bph.15182. doi:10.1111/bph.15182
46. Liu Y-C, Zou X-B, Chai Y-F, Yao Y-M. Macrophage Polarization in Inflammatory Diseases. *Int J Biol Sci* (2014) **10**:520–529. doi:10.7150/ijbs.8879
47. Atri C, Guerfali FZ, Laouini D. Role of Human Macrophage Polarization in Inflammation during Infectious Diseases. *Int J Mol Sci* (2018) **19**: doi:10.3390/ijms19061801
48. Stearns-Kurosawa DJ, Osuchowski MF, Valentine C, Kurosawa S, Remick DG. The Pathogenesis of Sepsis. *Annu Rev Pathol* (2011) **6**:19. doi:10.1146/ANNUREV-PATHOL-011110-130327
49. Ní Gabhann J, Hams E, Smith S, Wynne C, Byrne JC, Brennan K, Spence S, Kissenpfennig A, Johnston JA, Fallon PG, et al. Btk Regulates Macrophage Polarization in Response to Lipopolysaccharide. *PLoS One* (2014) **9**:e85834. doi:10.1371/journal.pone.0085834
50. Shen Y, Song J, Wang Y, Chen Z, Zhang L, Yu J, Zhu D, Zhong M. M2 macrophages promote pulmonary endothelial cells regeneration in sepsis-induced acute lung injury. *Ann Transl Med* (2019) **7**: doi:10.21037/ATM.2019.02.47
51. Li X, Mu G, Song C, Zhou L, He L, Jin Q, Lu Z. Role of M2 Macrophages in Sepsis-Induced Acute Kidney Injury. *SHOCK* (2018) **50**:233–239. doi:10.1097/SHK.0000000000001006
52. Chen J, Kieswich JE, Chiazza F, Moyes AJ, Gobbetti T, Purvis GSD, Salvatori DCF, Patel NSA, Perretti M, Hobbs AJ, et al. IκB Kinase Inhibitor Attenuates Sepsis-Induced Cardiac Dysfunction in CKD. *J Am Soc Nephrol* (2017) **28**:94–105. doi:10.1681/ASN.2015060670
53. Chaudhry H, Zhou J, Zhong Y, Ali MM, McGuire F, Nagarkatti PS, Nagarkatti M. Role of cytokines as a double-edged sword in sepsis. *In Vivo* (2013) **27**:669–84.
54. Bozza FA, Salluh JI, Japiassu AM, Soares M, Assis EF, Gomes RN, Bozza MT, Castro-Faria-Neto HC, Bozza PT. Cytokine profiles as markers of disease severity in sepsis: a multiplex analysis. *Crit Care* (2007) **11**:R49. doi:10.1186/CC5783
55. Liu X, Pichulik T, Wolz O-O, Dang T-M, Stutz A, Dillen C, Delmiro Garcia M, Kraus H, Dickhöfer S, Daiber E, et al. Human NACHT, LRR, and PYD domain–containing protein 3 (NLRP3) inflammasome activity is regulated by and potentially targetable through Bruton tyrosine kinase. *J Allergy Clin Immunol* (2017) **140**:1054-1067.e10. doi:10.1016/J.JACI.2017.01.017
56. Kumar V. Inflammasomes: Pandora's box for sepsis. *J Inflamm Res* (2018) **11**:477–502. doi:10.2147/JIR.S178084
57. Fu Q, Wu J, Zhou X-Y, Ji M-H, Mao Q-H, Li Q, Zong M-M, Zhou Z-Q, Yang J-J. NLRP3/Caspase-1 Pathway-Induced Pyroptosis Mediated Cognitive Deficits in a Mouse Model of Sepsis-Associated Encephalopathy. *Inflammation* (2019) **42**:306–318. doi:10.1007/s10753-018-0894-4

58. Lee S, Nakahira K, Dalli J, Siempos II, Norris PC, Colas RA, Moon J-S, Shinohara M, Hisata S, Howrylak JA, et al. NLRP3 Inflammasome Deficiency Protects against Microbial Sepsis via Increased Lipoxin B $_4$ Synthesis. *Am J Respir Crit Care Med* (2017) **196**:713–726. doi:10.1164/rccm.201604-0892OC
59. Van Wyngene L, Vandewalle J, Libert C. Reprogramming of basic metabolic pathways in microbial sepsis: therapeutic targets at last? *EMBO Mol Med* (2018) **10**: doi:10.15252/emmm.201708712
60. Yamaguchi J, Kinoshita K, Ihara S, Furukawa M, Sakurai A. The Clinical Significance of Low Serum Arachidonic Acid in Sepsis Patients with Hypoalbuminemia. *Intern Med* (2018) **57**:1833–1840. doi:10.2169/internalmedicine.9124-17
61. Yost CC, Weyrich AS, Zimmerman GA. The platelet activating factor (PAF) signaling cascade in systemic inflammatory responses. *Biochimie* (2010) **92**:692–7. doi:10.1016/j.biochi.2010.02.011
62. Baker RR. Lipid Acetylation Reactions and the Metabolism of Platelet-Activating Factor. *Neurochem Res* (2000) **25**:667–683. doi:10.1023/A:1007567205078
63. Tutunchi H, Saghafi-Asl M, Ostadrahimi A. A systematic review of the effects of oleoylethanolamide, a high-affinity endogenous ligand of PPAR-α, on the management and prevention of obesity. *Clin Exp Pharmacol Physiol* (2020) **47**:543–552. doi:10.1111/1440-1681.13238
64. Chang S, Kim Y-H, Kim Y-J, Kim Y-W, Moon S, Lee YY, Jung JS, Kim Y, Jung H-E, Kim T-J, et al. Taurodeoxycholate Increases the Number of Myeloid-Derived Suppressor Cells That Ameliorate Sepsis in Mice. *Front Immunol* (2018) **9**:1984. doi:10.3389/fimmu.2018.01984
65. Li F, Zhang B, Duan S, Qing W, Tan L, Chen S, Wang Y, Li D, Yang J, Tong J, et al. Small dose of L-dopa/Benserazide hydrochloride improved sepsis-induced neuroinflammation and long-term cognitive dysfunction in sepsis mice. *Brain Res* (2020) **1737**:146780. doi:10.1016/j.brainres.2020.146780
66. Stone MD, Nelsestuen GL. Efficacy of Soluble Phospholipids in the Prothrombinase Reaction†. (2005) doi:10.1021/BI047655N
67. Zhang Y, Meng H, Ma R, He Z, Wu X, Cao M, Yao Z, Zhao L, Li T, Deng R, et al. Circulating Microparticles, Blood Cells, and Endothelium Induce Procoagulant Activity in Sepsis Through Phosphatidylserine Exposure. *SHOCK* (2016) **45**:299–307. doi:10.1097/SHK.0000000000000509
68. Audrito V, Messana VG, Deaglio S. NAMPT and NAPRT: Two Metabolic Enzymes With Key Roles in Inflammation. *Front Oncol* (2020) **10**: doi:10.3389/FONC.2020.00358
69. Tsalik EL, Willig LK, Rice BJ, van Velkinburgh JC, Mohney RP, McDunn JE, Dinwiddie DL, Miller NA, Mayer ES, Glickman SW, et al. Renal systems biology of patients with systemic inflammatory response syndrome. *Kidney Int* (2015) **88**:804–14. doi:10.1038/ki.2015.150
70. Callahan LA, Supinski GS. Sepsis-induced myopathy. *Crit Care Med* (2009) **37**:S354. doi:10.1097/CCM.0B013E3181B6E439
71. Baranwal AK, Deepthi G, Rohit MK, Jayashree M, Angurana SK, Kumar-M P. Longitudinal Study of CPK-MB and Echocardiographic Measures of Myocardial Dysfunction in Pediatric Sepsis: Are Patients with Shock Different from Those without? *Indian J Crit Care Med* (2020) **24**:109–115. doi:10.5005/jp-journals-10071-23340
72. Miller SG, Hafen PS, Brault JJ. Increased Adenine Nucleotide Degradation in Skeletal Muscle Atrophy. *Int J Mol Sci* (2019) **21**:88. doi:10.3390/ijms21010088
73. Vanmassenhove J, Lameire N, Dhondt A, Vanholder R, Van Biesen W. Prognostic

robustness of serum creatinine based AKI definitions in patients with sepsis: a prospective cohort study. *BMC Nephrol* (2015) **16**:112. doi:10.1186/s12882-015-0107-4

74. Lögters TT, Laryea MD, Altrichter J, Sokolowski J, Cinatl J, Reipen J, Linhart W, Windolf J, Scholz M, Wild M. Increased plasma kynurenine values and kynurenine-tryptophan ratios after major trauma are early indicators for the development of sepsis. *Shock* (2009) **32**:29–34. doi:10.1097/SHK.0b013e31819714fa

75. Murtagh F, Legendre P. Ward's Hierarchical Agglomerative Clustering Method: Which Algorithms Implement Ward's Criterion? *J Classif* (2014) **31**:274–295. doi:10.1007/s00357-014-9161-z

Figures

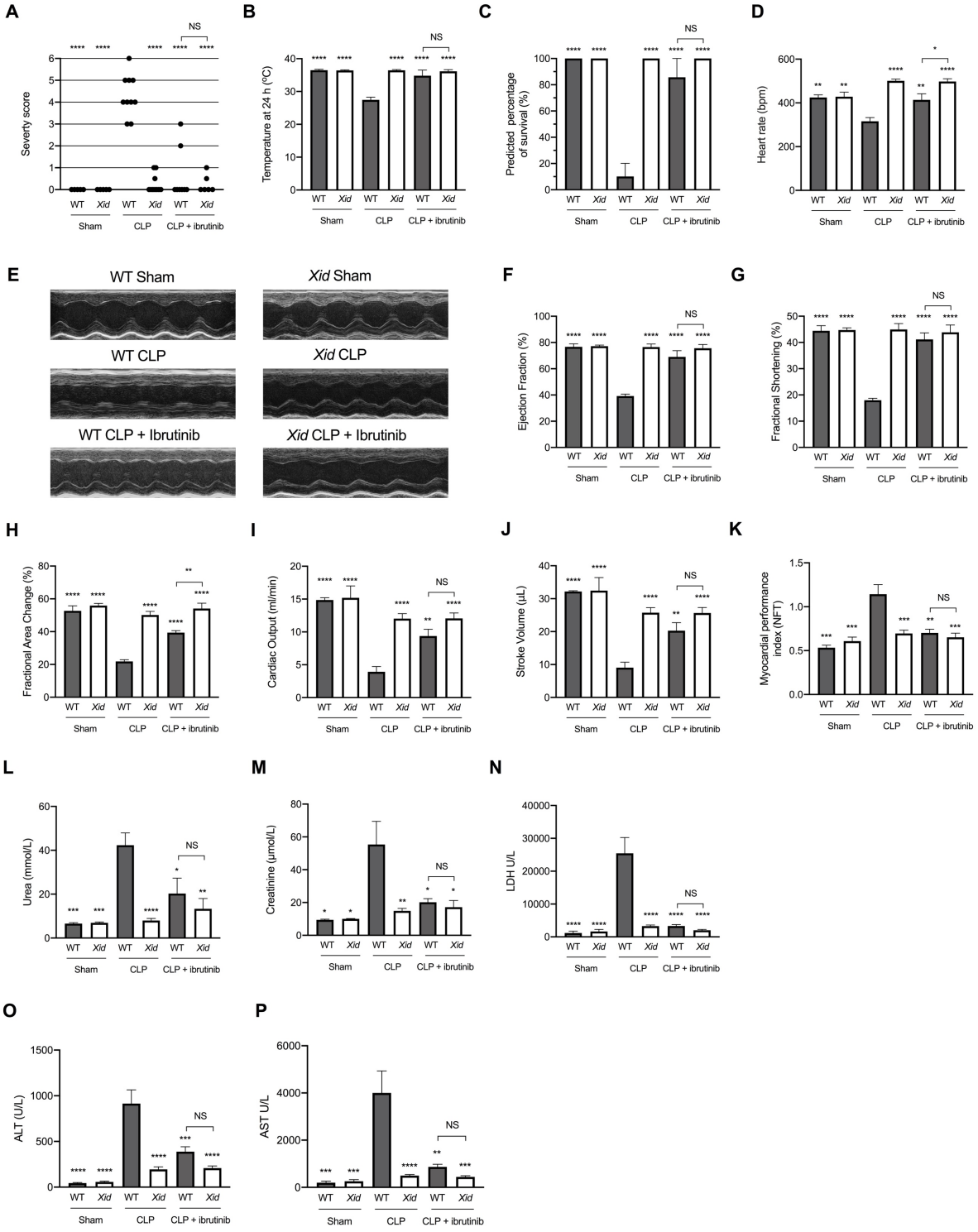

Figure 1. *Xid* mice are protected from sepsis-induced multiple organ failure. WT and *Xid* mice were randomly selected to undergo sham or CLP surgery, 1 h later ibrutinib (30 mg/kg) was administered intravenously. At 24 h after CLP, cardiac function was assessed by echocardiography and parameters of renal and liver function were assessed in serum. **(A)** Severity Score 24 h after CLP. **(B)** Temperature 24 h after CLP (ºC). **(C)** Predicted percentage of survival (%). **(D)** Heart rate 24 h after CLP (bmp). **(E)** Representative m-mode images. **(F)**

995 Ejection Fraction (%). **(G)** Fractional shortening (%). **(H)** Fractional area change (%). **(I)**
996 Cardiac output (ml/min). **(J)** Stroke volume (μL). **(K)** Myocardial performance index (NFT).
997 **(L)** Urea (mmol/L). **(M)** Creatinine (μmol/L). **(N)** Lactate dehydrogenase (U/L). **(O)** ATL
998 (U/L). **(P)** AST (U/L). The following groups were studied WT sham ($n = 5$), *Xid* sham ($n = 5$),
999 WT-CLP ($n = 10$), *Xid*-CLP ($n = 10$), WT-CLP + ibrutinib ($n = 8$) and *Xid*-CLP + ibrutinib (n
1000 $= 6$). Data are expressed as mean ± SEM and analysed by one-way ANOVA with a Bonferroni
1001 post hoc test. *$P < 0.05$, **$P < 0.01$, ***$P < 0.001$ ****$P < 0.0001$ *versus* WT-CLP.
1002

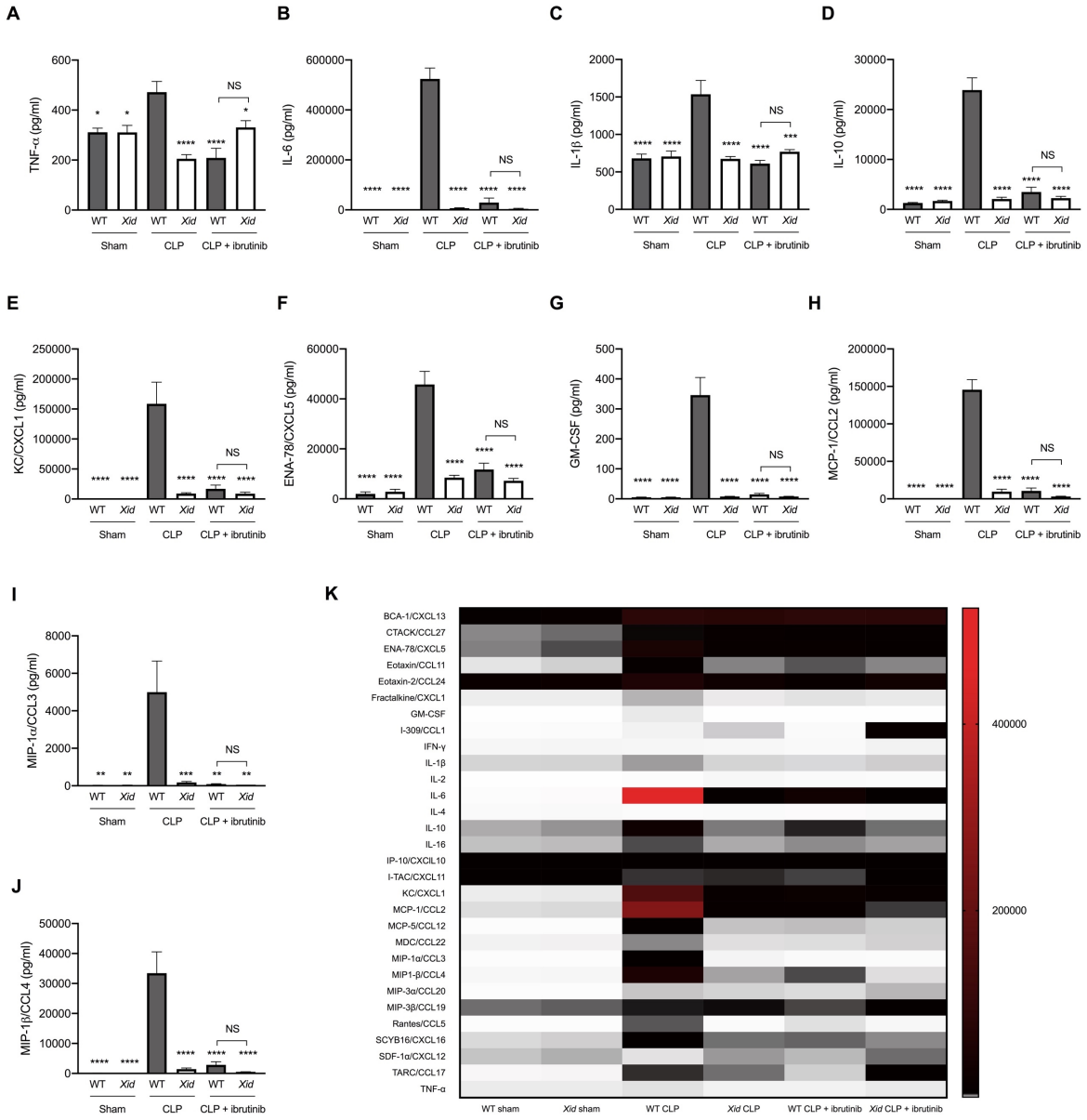

Figure 2. *Xid* mice do not present with systemic inflammation after polymicrobial sepsis. Mice underwent sham or CLP surgery, 24 h later cytokines and chemokines were assessed in serum. **(A)** TNF-α serum concentration (pg/ml). **(B)** IL-6 serum concentration (pg/ml). **(C)** IL-1β serum concentration (pg/ml). **(D)** IL-10 serum concentration (pg/ml). **(E)** KC/CXCL1 serum concentration (pg/ml). **(F)** ENA-78/CXCL5 serum concentration (pg/ml). **(G)** GM-CSF serum concentration (pg/ml). **(H)** MCP-1/CCL2 serum concentration (pg/ml). **(I)** MIP-1α/CCL3 serum concentration (pg/ml). **(J)** MIP-1β/CCL4 serum concentration (pg/ml). **(K)** Heat-map of 31 cytokines/chemokines serum concentration (pg/ml). The following groups were studied WT sham ($n = 5$), *Xid* sham ($n = 5$), WT-CLP ($n = 10$), *Xid*-CLP ($n = 10$), WT-CLP + ibrutinib ($n = 8$) and *Xid*-CLP + ibrutinib ($n = 6$). Data are expressed as mean ± SEM and analysed by one-way ANOVA with a Bonferroni post hoc test. $^{*}P < 0.05$, $^{**}P < 0.01$, $^{***}P < 0.001$ $^{****}P < 0.0001$ *versus* WT-CLP.

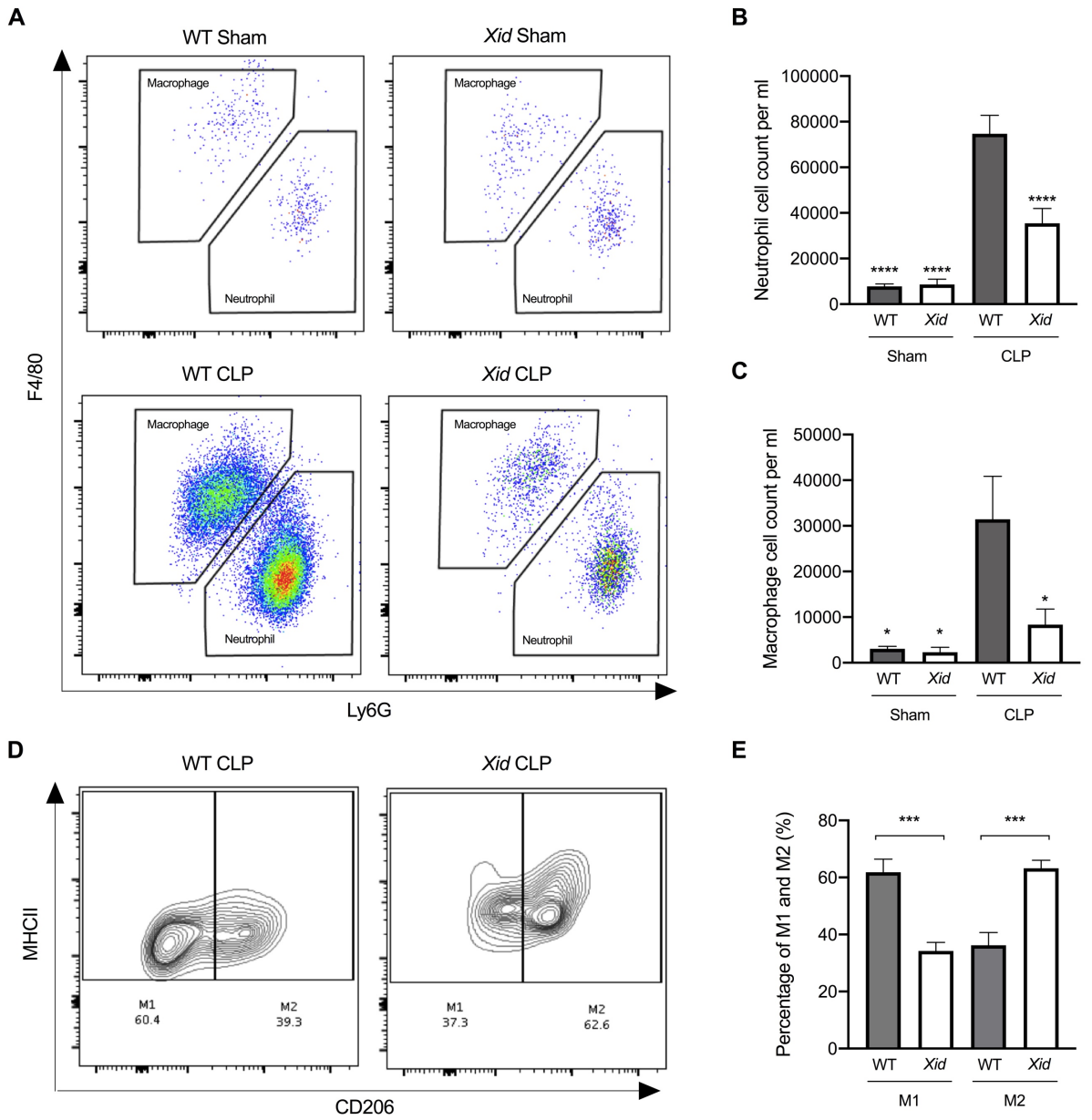

Figure 3. *Xid* mice have fewer infiltrating immune cells in the peritoneum and enhanced polarisation to M2 macrophages. Mice underwent sham or CLP surgery, 24 h later peritoneal lavage fluid was analysed. **(A)** Scattergrams illustrating macrophage (identified as $F4/80^{+}Ly6G^{-}$) and neutrophils (identified as $F4/80^{-}Ly6G^{+}$). **(B)** Peritoneal neutrophil ($F4/80^{-}Ly6G^{+}$) cell count per ml. **(C)** Peritoneal macrophage ($F4/80^{+}Ly6G^{-}$) cell count per ml. **(D)** Contour plot illustrating percentage of M1 and M2 macrophages in WT and *Xid* mice, M1 identified as $MHCII^{+}CD206^{-}$ and M2 identified as $MHCII^{+}CD206^{+}$. **(E)** Percentage of M1 and M2 macrophages in WT mice and *Xid* mice (%). The following groups were studied WT sham ($n = 5$), *Xid* sham ($n = 5$), WT-CLP ($n = 10$) and *Xid*-CLP ($n = 10$). Data are expressed as mean ± SEM and analysed by one-way ANOVA with a Bonferroni post hoc test. $^{*}P < 0.05$, $^{***}P < 0.001$ $^{****}P < 0.0001$ *versus* WT-CLP.

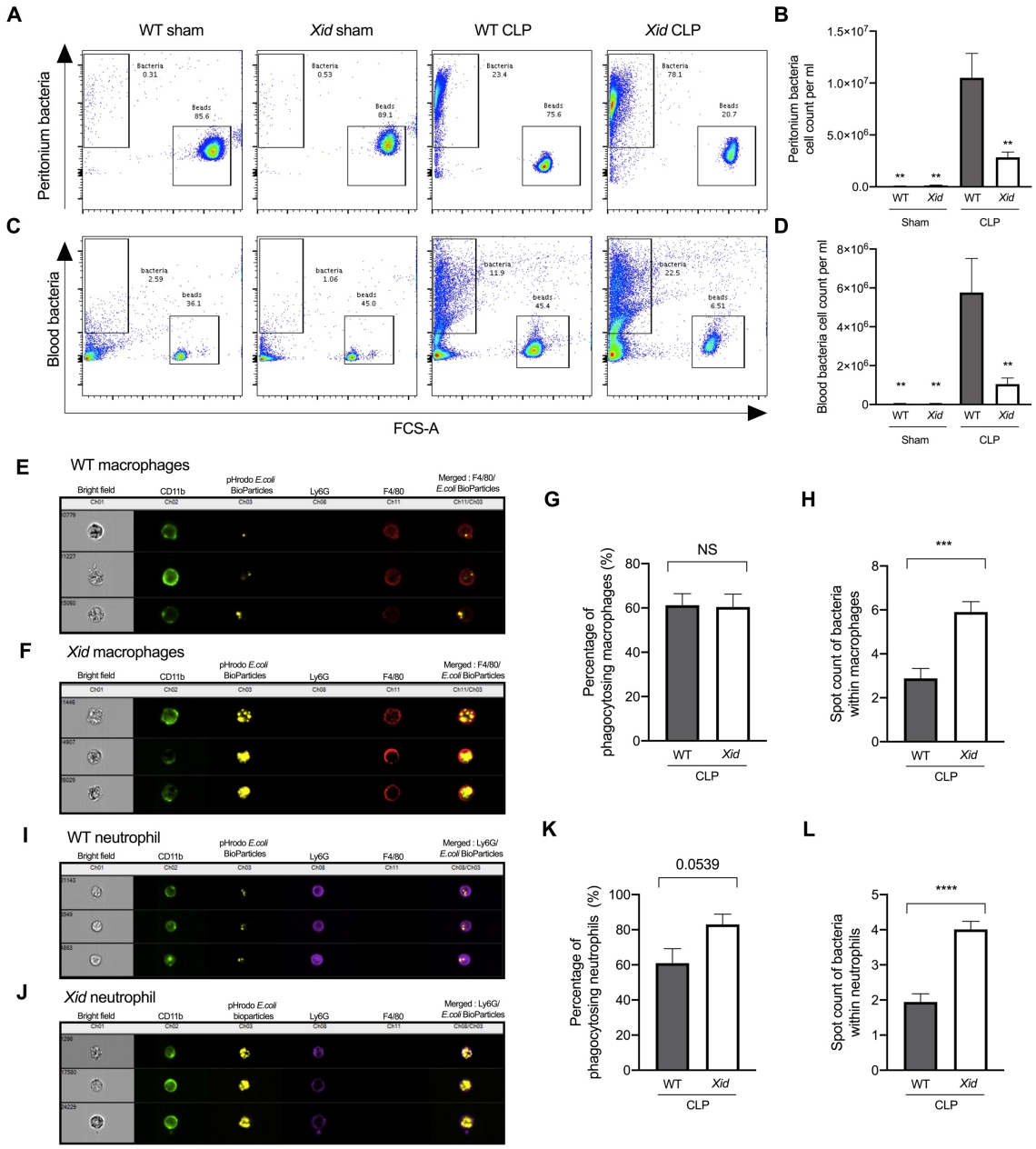

Figure 4. *Xid* mice result in enhanced bacterial clearance in peritoneum and blood due to increased phagocytosis in sepsis. Mice underwent sham or CLP surgery, 24 h later peritoneal lavage fluid and blood were analysed. Macrophages identified as (CD11b$^+$, F4/80$^+$ and Ly6G$^-$) and neutrophils identified as (CD11b$^+$, F4/80$^-$ and Ly6G$^+$) **(A)** Representative images of peritoneal bacteria cell count. **(B)** Peritoneum bacteria cell count per ml. **(C)** Representative images of blood bacteria cell count. **(D)** Blood bacteria cell count per ml. **(E)** Representative images of WT-CLP macrophages phagocytosis on the imagestream. **(F)** Representative images of *Xid*-CLP macrophages phagocytosis on the imagestream. **(G)** Percentage of phagocytosing macrophages (%). **(H)** Average number of pHrodo red *E.coli* BioParticles within macrophages. **(I)** Representative images of WT-CLP neutrophil phagocytosis on the imagestream. **(J)** Representative images of *Xid*-CLP neutrophil phagocytosis on the imagestream. **(K)** Percentage of phagocytosing neutrophils (%). **(L)** Average number of pHrodo red *E.coli* BioParticles within neutrophils. The following groups were studied WT sham ($n = 5$), *Xid* sham ($n = 5$,) WT-CLP ($n = 10$) and *Xid*-CLP ($n = 10$). Data are expressed as mean ± SEM and analysed by one-way ANOVA with a Bonferroni post hoc test. $^{**}P < 0.01$, $^{***}P < 0.001$ $^{****}P < 0.0001$ *versus* WT-CLP.

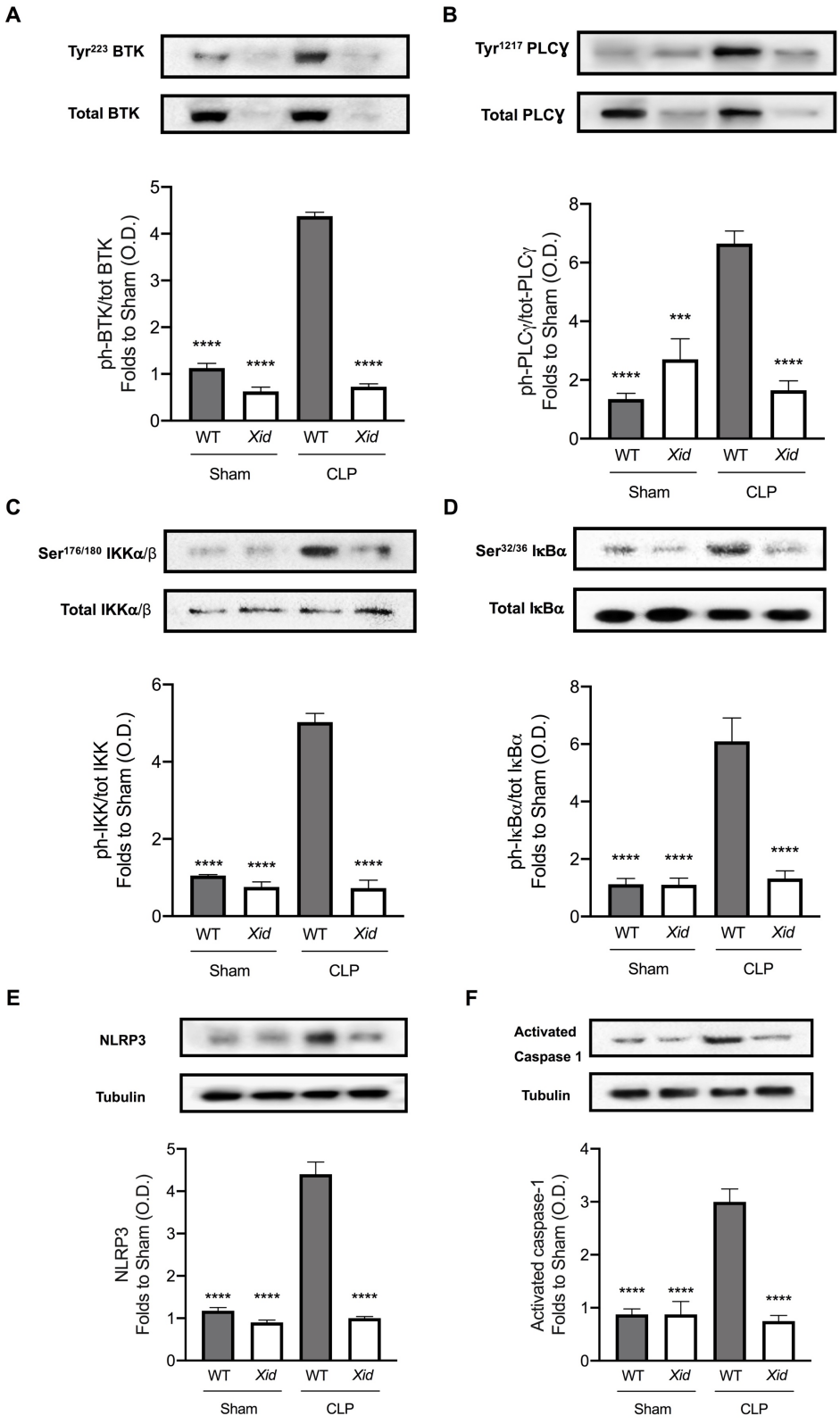

Figure 5. BTK, NF-κB and NLRP3 inflammasome are not activated in *Xid* mice after polymicrobial sepsis. Mice underwent sham-operated or CLP surgery and 24 h later signalling events in the cardiac tissue were assessed. Densitometric analysis of the bands is expressed as relative optical density (O.D.) of **(A)** phosphorylation of BTK at Tyr^{223} corrected for the corresponding total BTK and normalized using the related sham bands. **(B)** Phosphorylation of PLCγ at Tyr^{1217} corrected for the corresponding total PLCγ and normalised using the related

sham bands. **(C)** Phosphorylation of IKKα/β at $Ser^{176/180}$ corrected for the corresponding total IKKα/β and normalised using the sham related bands. **(D)** Phosphorylation of IκBα at $Ser^{32/36}$ corrected for the corresponding total IκBα and normalised using the related sham band. **(E)** NLRP3 activation, corrected against tubulin and normalized using the sham related bands. **(F)** Pro-caspase-1 against activated caspase-1 and normalized using the sham related bands. The following groups were studied WT sham ($n = 4$), *Xid* sham ($n = 4$), WT-CLP ($n = 4$) and *Xid*-CLP ($n = 4$). Data are expressed as mean ± SEM and analysed by one-way ANOVA with a Bonferroni post hoc test. ***$P < 0.001$ ****$P < 0.0001$ *versus* WT-CLP.

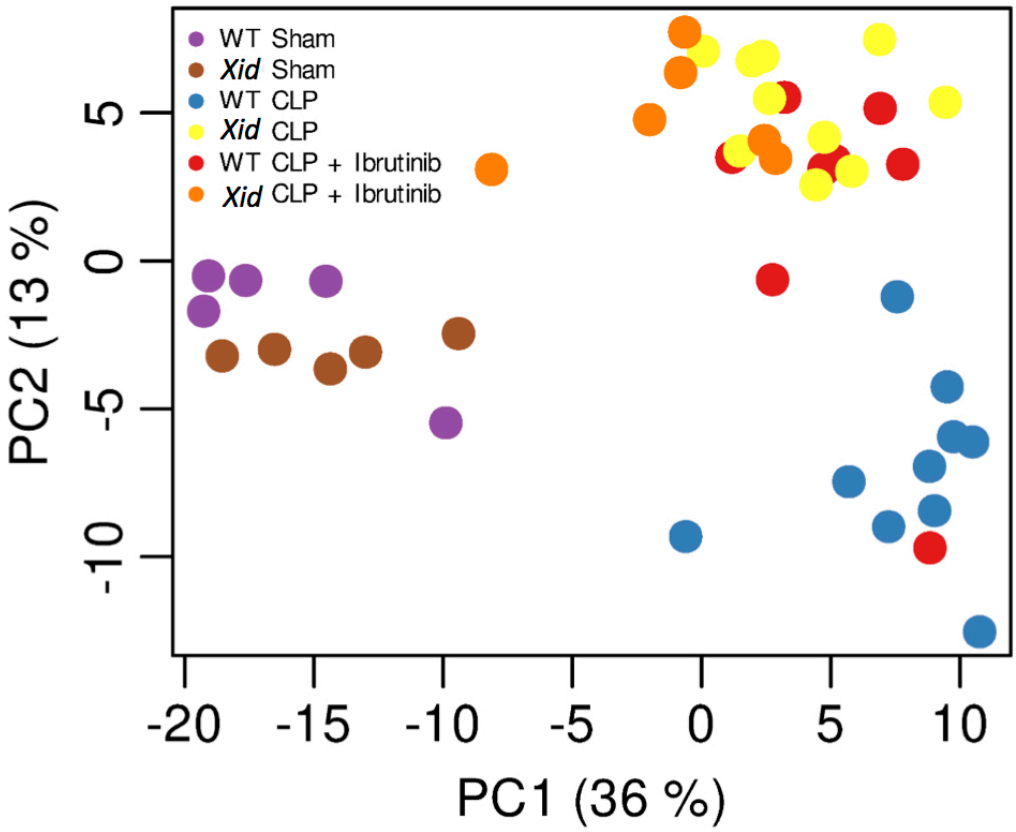

Figure 6. Principal component analysis (PCA). Principal component analysis (PCA) of the normalised and scaled metabolome data. Plot shows first two principal components (PC), which account for almost half of the total variance in the data set. Variance between replicates is far less than between different experimental conditions. Contrasts between main experimental conditions are visible in the shown PCs. Each dot represents a sample and each colour represents a mice group.

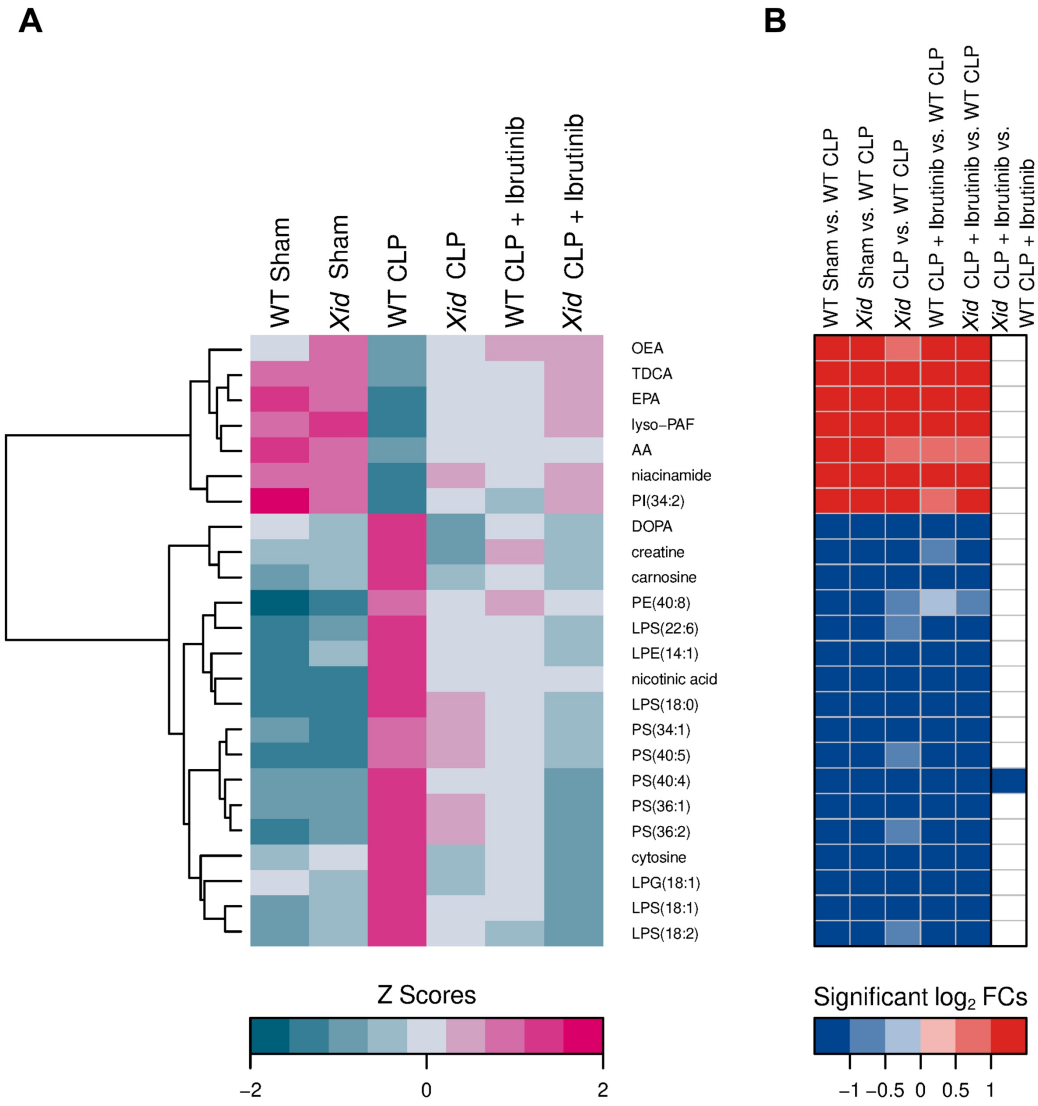

Figure 7. Heatmap of significant restored metabolites in the groups XID CLP, WT CLP + Ibrutinib and XID CLP + Ibrutinib. (A) Hierarchical clustered z score heatmaps showed significantly changed analytes and **(B)** log2 fold change heatmaps showed their significant log2 fold changes for selected groupwise comparisons. The heatmap shows analytes which, compared to the WT CLP group ($n = 10$), restored in all three groups (*Xid*-CLP ($n = 10$), WT-CLP + ibrutinib ($n = 8$) and *Xid*-CLP + ibrutinib ($n = 6$)) to the level of the two sham groups (WT Sham ($n = 5$), *Xid* Sham ($n = 5$)). Each column in a z score heatmap represented the mean value of all animals in a group, each column in a log2 fold change heatmap represented a groupwise comparison and each row defined an analyte. Analytes were hierarchically clustered using Ward's minimum variance method (75) and an euclidian distance between log2 fold changes. Dendrograms provide information about distances between clusters. AA: arachidonic acid, AEA: arachidonoylethanolamide, DHA: docosahexaenoic acid, DOPA: dihydroxyphenylalanine, EPA: eicosapentaenoic acid, LPE: lysophosphatidylethanolamine, LPG: lysophosphatidylglycerol, LPS: lysophosphatidylserine, lyso-PAF: lyso-platelet activating factor, OEA: oleoylethanolamine, PE: phosphatidylethanolamine, PI: phosphatidylinositol, PS: phosphatidylserine, TDCA: taurodeoxycholic acid.

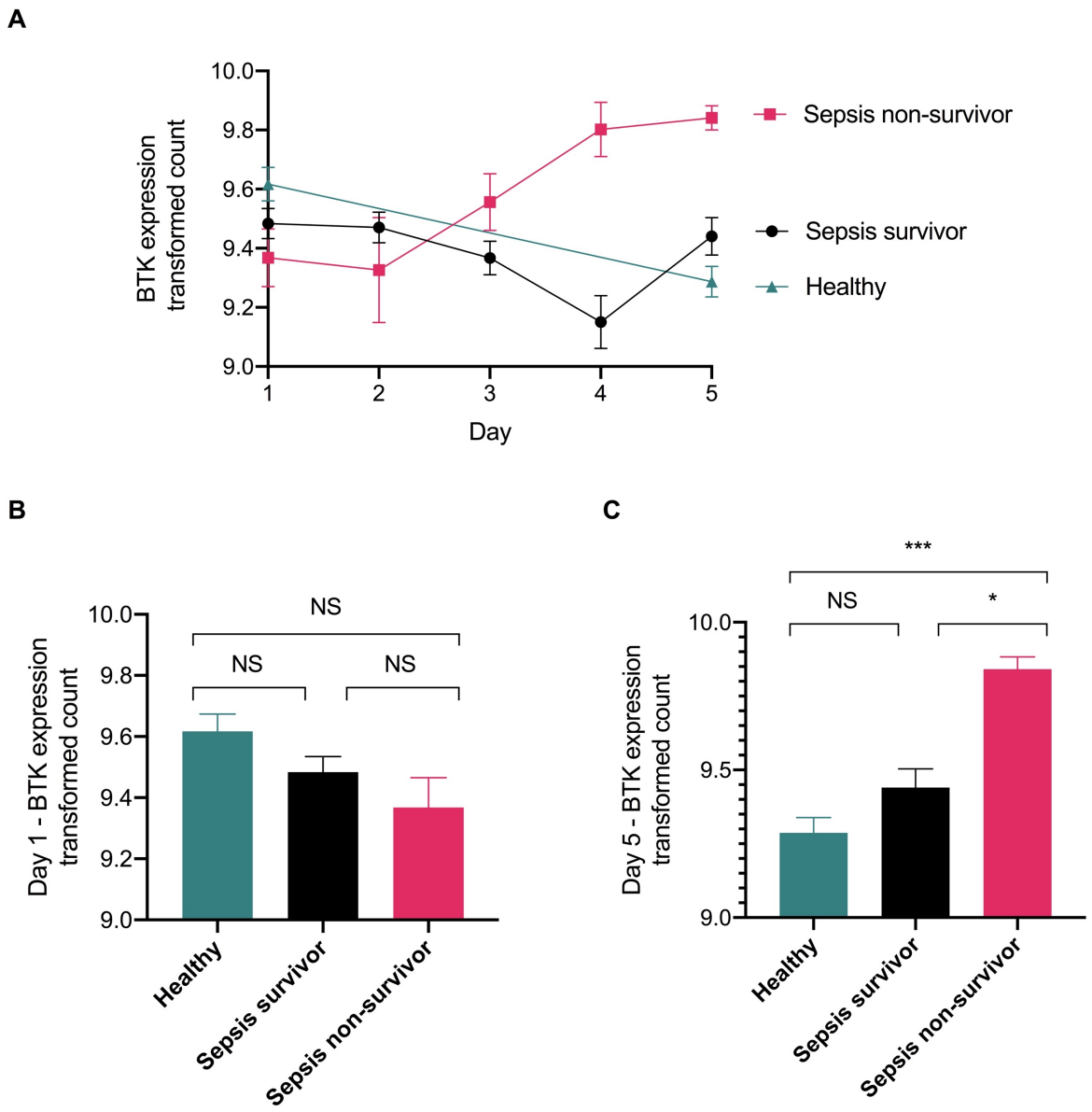

1085

1086 **Figure 8. Expression of BTK is increased in whole human blood of septic non-survivor's**
1087 Original data was obtained from the gene expression omnibus under dataset number GDS4971
1088 which was published by Parnell GP *et al*. Whole blood of patients confirmed with sepsis (and
1089 healthy participants) over a 5-day time course. RNA was extracted from whole blood and
1090 analysed for gene expression via microarray Illumina GenomeStudio V2010.3. Three groups
1091 were collected, healthy participants, septic survivors and septic non-survivors. **(A)** Time course
1092 of BTK expression. **(B)** Day 1 BTK expression. **(C)** Day 5 BTK expression. Data was
1093 reanalysed looking for expression of BTK gene in their dataset and generated the figure using
1094 the software R, gene expression was quantile normalization and log transformation of the data
1095 was applied. Significance was determined by one-way ANOVA followed by Bonferroni post
1096 hoc test and a value of $*P < 0.05$ and $***P < 0.001$ were considered significant. Data are
1097 expressed as mean ± SEM. Day 1 healthy (n = 18), septic survivors (n = 26), septic non-
1098 survivors (n = 9). Day 2 septic survivors (n = 24), septic non-survivors (n = 7). Day 3 septic
1099 survivors (n = 22), septic non-survivors (n = 7). Day 4 septic survivors (n = 13), septic non-
1100 survivors (n = 5). Day 5 healthy (n = 18), septic survivors (n = 11), septic non-survivors (n =
1101 3).

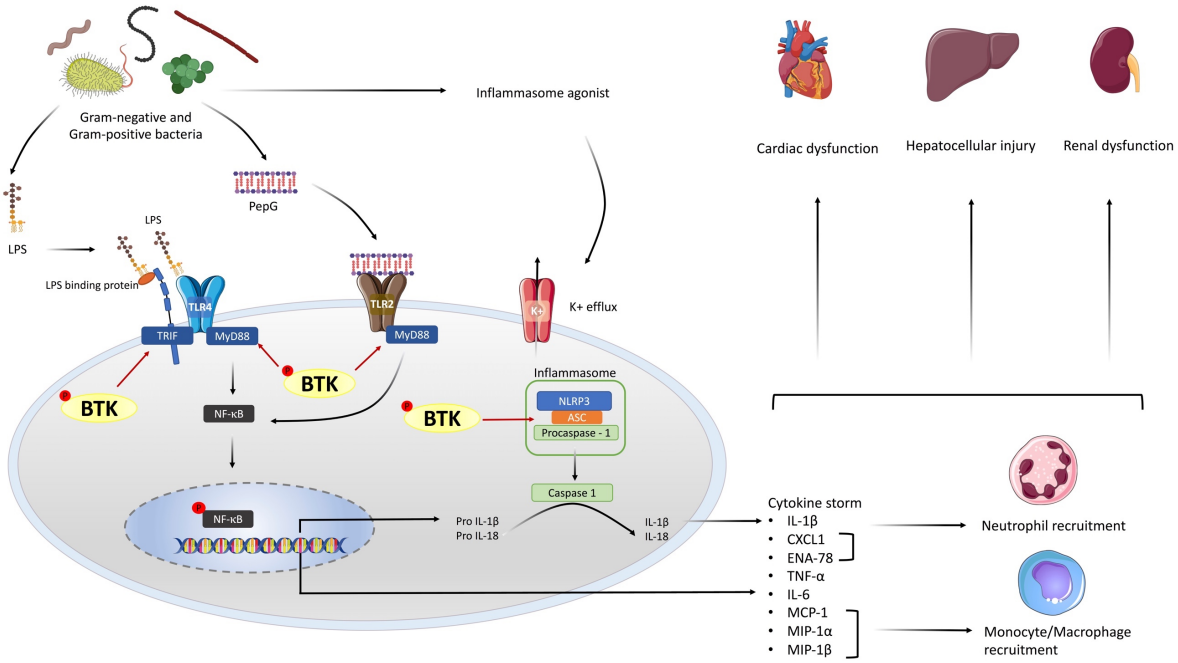

Figure 9. Schematic diagram representing the role of Bruton's tyrosine kinase (BTK) in the pathophysiology of sepsis. LPS is released from Gram-negative bacteria which activate the TLR4 signalling pathway and the release of PepG from Gram-positive bacteria activate the TLR2 signalling pathway. BTK is involved in the activation of TLR4 and TLR2 by binding to MyD88 and TRIF thus activating their representative signalling cascades. The activation of the MyD88 signalling pathway, leads to the activation of NF-κB and the production of pro-inflammatory cytokines. Additionally, BTK activates the NLRP3 inflammasome by binding to the ASC component of the inflammasome. Once active the NLRP3 inflammasome cleaves pro-IL-1β to active IL-1β. The production of chemokines from NF-κB activation results in the recruitment of neutrophils and macrophages. Excessive inflammation from the cytokine storm and innate immune cells results in multiple organ failure/injury. The use of BTK inhibitors such as ibrutinib or acalabrutinib supress sepsis-induced inflammation and thus multiple-organ failure/injury.

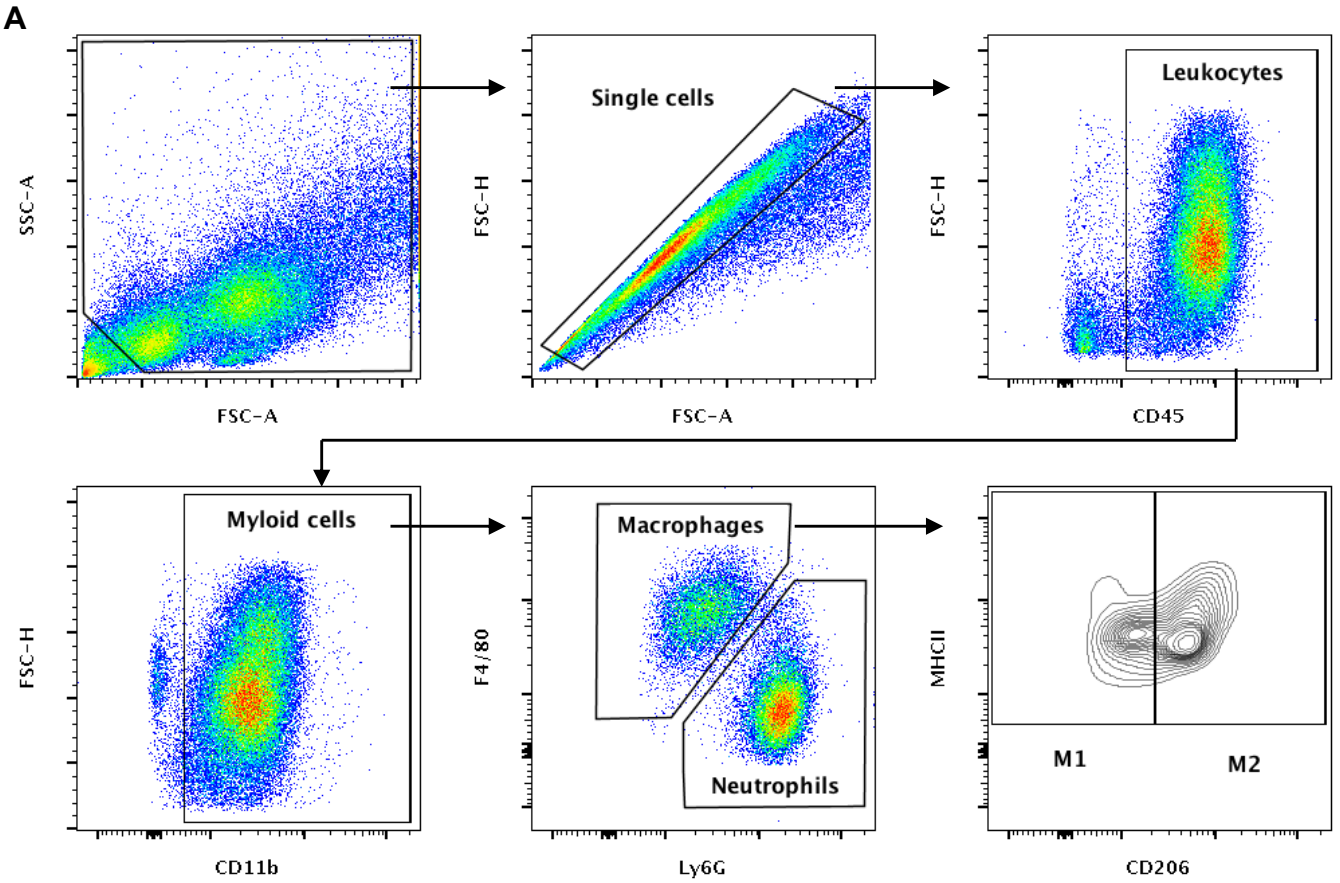

Figure S1. Flow cytometry gating strategy. Flow cytometry gating strategy of mouse peritoneal immune cells 24 h post-CLP.

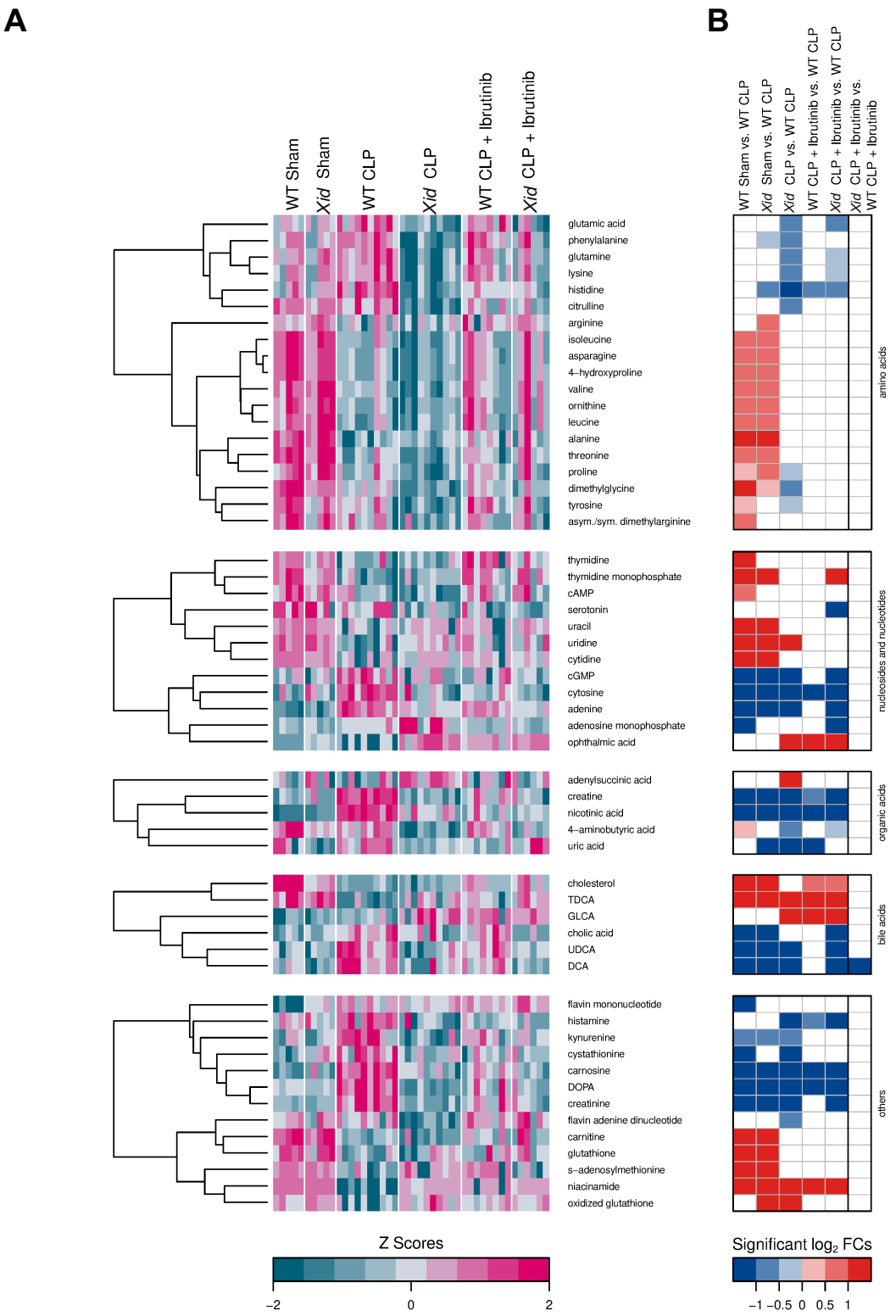

Figure S2. Heatmaps of primary metabolites. Hierarchical clustered z score heatmaps showed significantly changed primary metabolites (A) and log2 fold change heatmaps showed their significant log2 fold changes for selected groupwise comparisons (B). Each column in a z score heatmap represented an animal and each column in a log2 fold change heatmap represented a groupwise comparison and each row defined an analyte. Primary metabolites were divided in five groups: amino acids, nucleosides and nucleotides, organic acids, bile acids and others. Analytes were hierarchically clustered using Ward's minimum variance method and an euclidian distance between log2 fold changes. Dendrograms provide information about distances between clusters. cAMP: cyclic adenosine monophosphate, DOPA: dihydroxyphenylalanine, TDCA: taurodeoxycholic acid, UDCA: ursodeoxycholic acid, DCA: deoxycholic acid, GLCA: glycolithocholic acid, TCDCA: taurochenodeoxycholic acid.

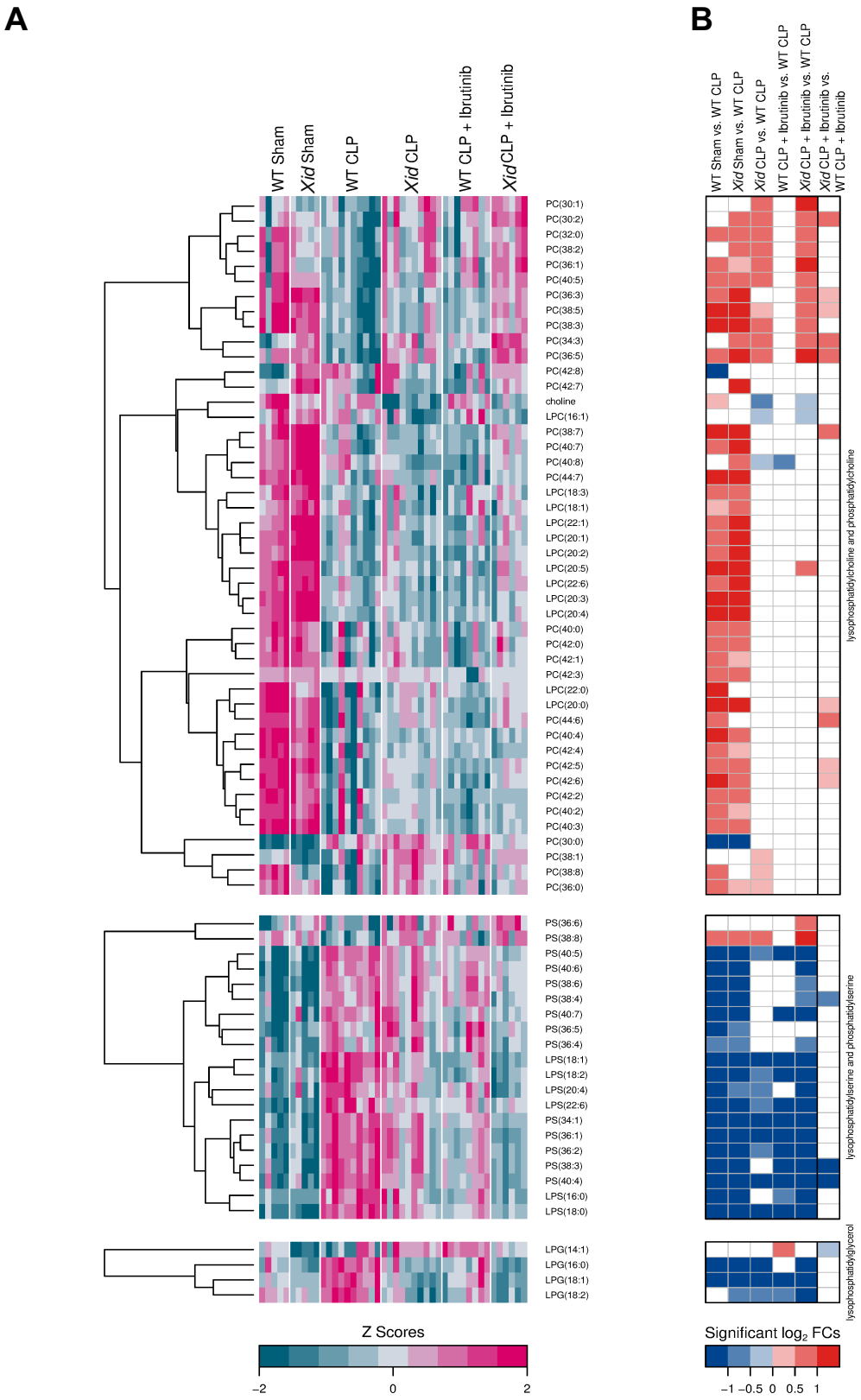

Figure S3. Heatmaps of phospholipids I. (A) Hierarchical clustered z score heatmaps showed significantly changed primary metabolites. **(B)** log2 fold change heatmaps showed their significant log2 fold changes for selected groupwise comparisons Each column in a z score heatmap represented an animal and each column in a log2 fold change heatmap represented a groupwise comparison and each row defined an analyte. Phospholipids were divided in LPC and PC, LPS and PS and LPG. Analytes were hierarchically clustered using Ward's minimum variance method and an euclidian distance between log2 fold changes. Dendrograms provide information about distances between clusters. LPC: lysophosphatidylcholine, PC: phosphatidylcholine, LPS: lysophosphatidylserine, PS: phosphatidylserine, LPG: lysophosphatidylglycerol.

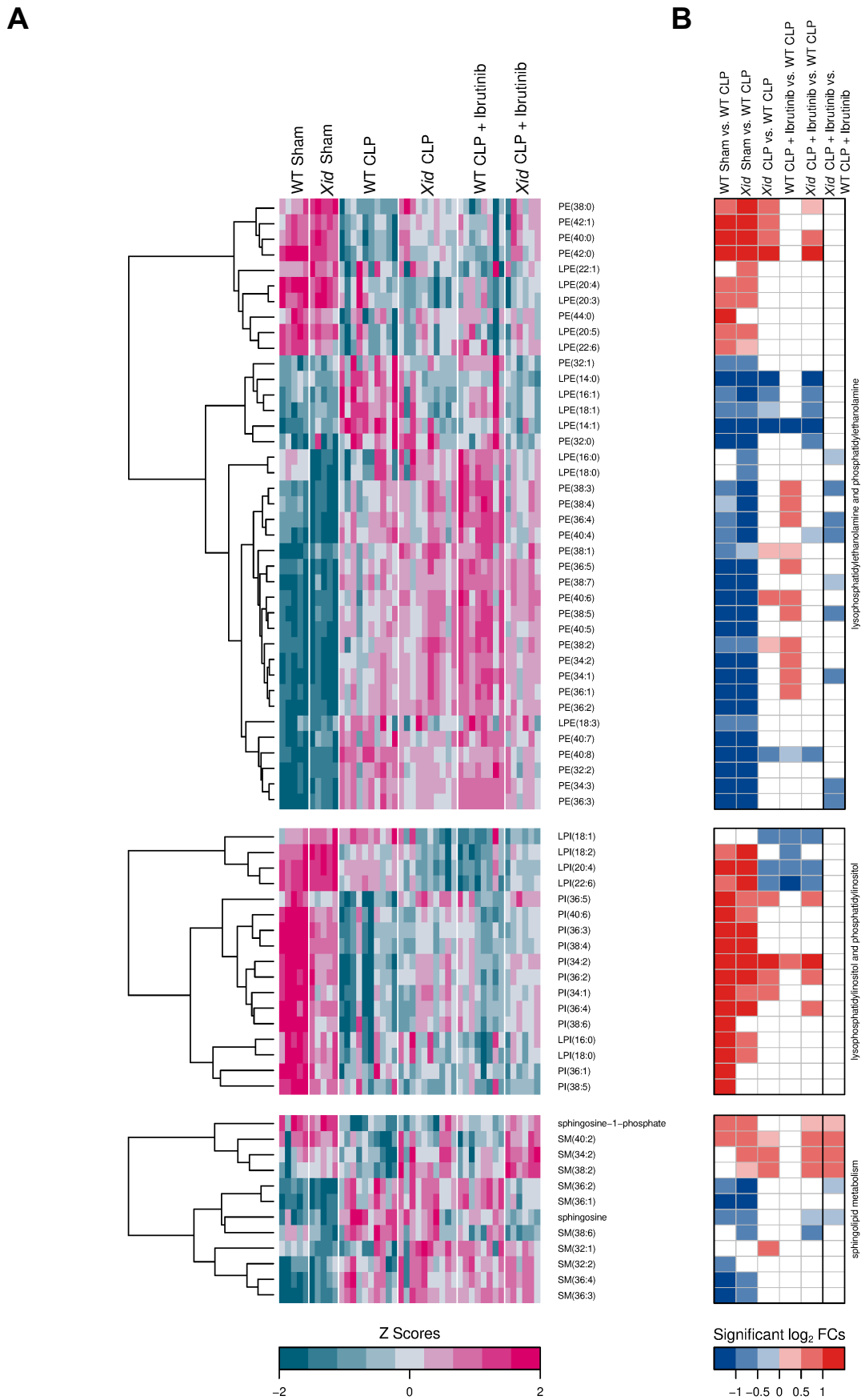

Figure S4. Heatmaps of phospholipids II. (A) Hierarchical clustered z score heatmaps showed significantly changed phospholipids. **(B)** log2 fold change heatmaps showed their significant log2 fold changes for selected groupwise comparisons Each column in a z score heatmap represented an animal and each column in a log2 fold change heatmap represented a groupwise comparison and each row defined an analyte. Phospholipids were divided in LPE and PE, LPI and PI and sphingolipid metabolism. Analytes were hierarchically clustered using Ward's minimum variance method and an euclidian distance between log2 fold changes. Dendrograms provide information about distances between clusters. LPE: lysophosphatidylethanolamine, PE: phosphatidylethanolamine, LPI: lysophosphatidylinositol, PI: phosphatidylinositol, SM: sphingomyelins.

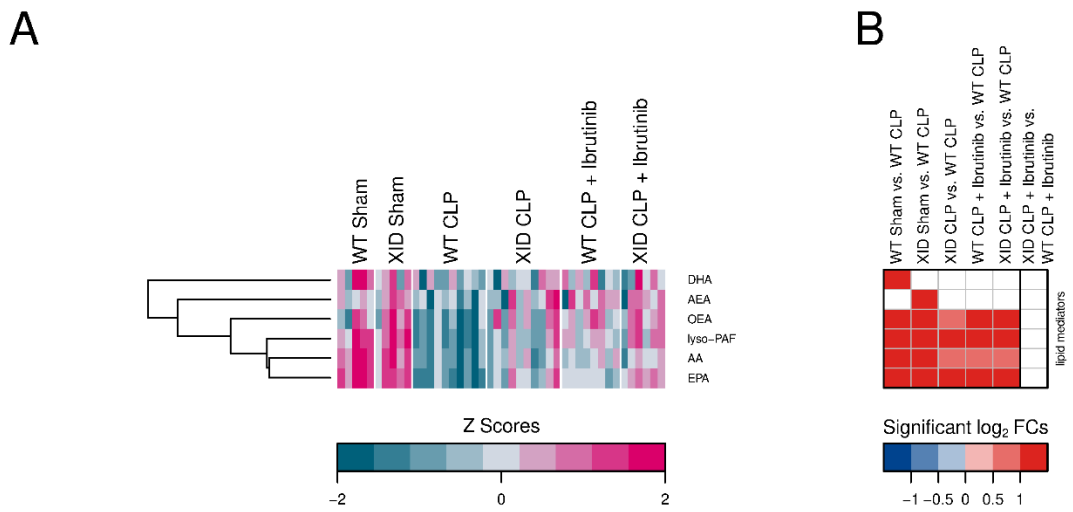

Figure S5. Heatmap of lipid mediators. (A) Hierarchical clustered z score heatmaps showed significantly changed lipid mediators. **(B)** log2 fold change heatmaps showed their significant log2 fold changes for selected groupwise comparisons. Each column in a z score heatmap represented an animal and each column in a log2 fold change heatmap represented a groupwise comparison and each row defined an analyte. Analytes were hierarchically clustered using Ward's minimum variance method and an euclidian distance between log2 fold changes. Dendrograms provide information about distances between clusters. AEA: arachidonoylethanolamide, AA: arachidonic acid, DHA: docosahexaenoic acid, EPA: eicosapentaenoic acid, lyso-PAF: lyso-platelet activating factor, OEA: oleoylethanolamine.

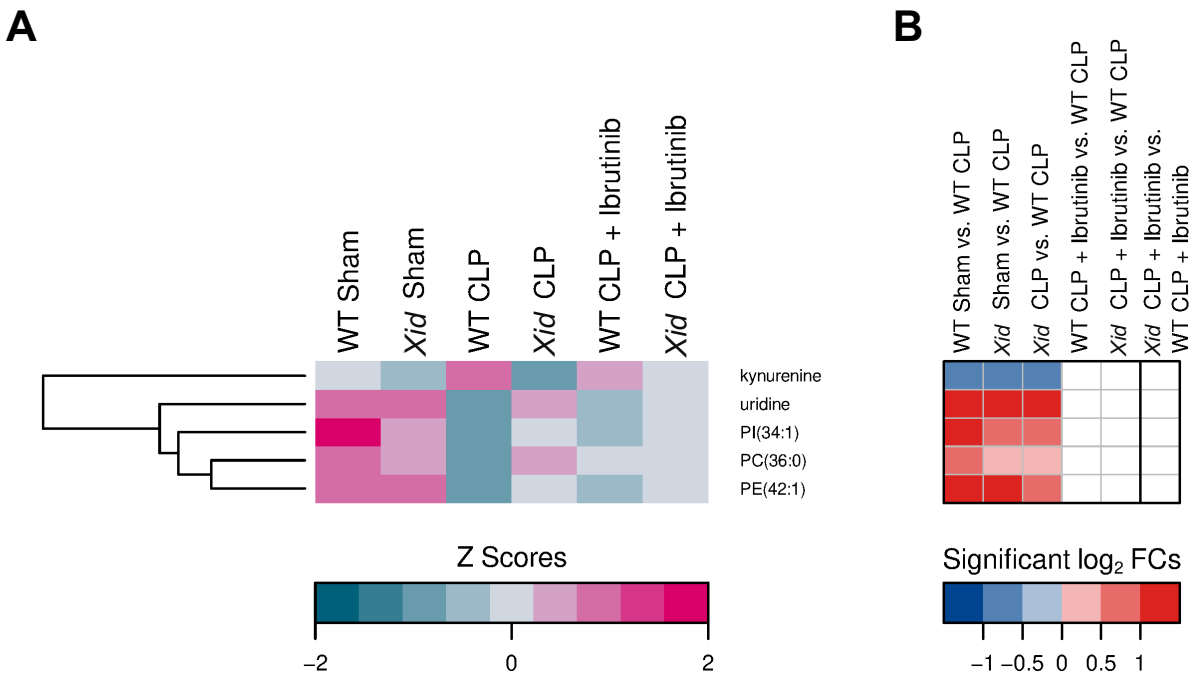

Figure S6. Heatmap of significant restored metabolites in the group *Xid*-CLP. (A) Hierarchical clustered z score heatmaps showed significantly changed metabolites. **(B)** log2 fold change heatmaps showed their significant log2 fold changes for selected groupwise comparisons. The heatmap shows metabolites which, compared to the WT-CLP group (n = 10), restored in the group *Xid*-CLP (n = 10), but not in the groups WT-CLP + Ibrutinib (n = 8) and *Xid*-CLP + Ibrutinib (n = 6) to the level of the two sham groups (WT Sham (n = 5), *Xid* Sham (n = 5)). Each column in a z score heatmap represented the mean value of all animals in a group, each column in a log2 fold change heatmap represented a groupwise comparison and each row defined an analyte. Analytes were hierarchically clustered using Ward's minimum variance method and an euclidian distance between log2 fold changes. Dendrograms provide information about distances between clusters. PC: phosphatidylcholine PE: phosphatidylethanolamine, PI: phosphatidylinositol.

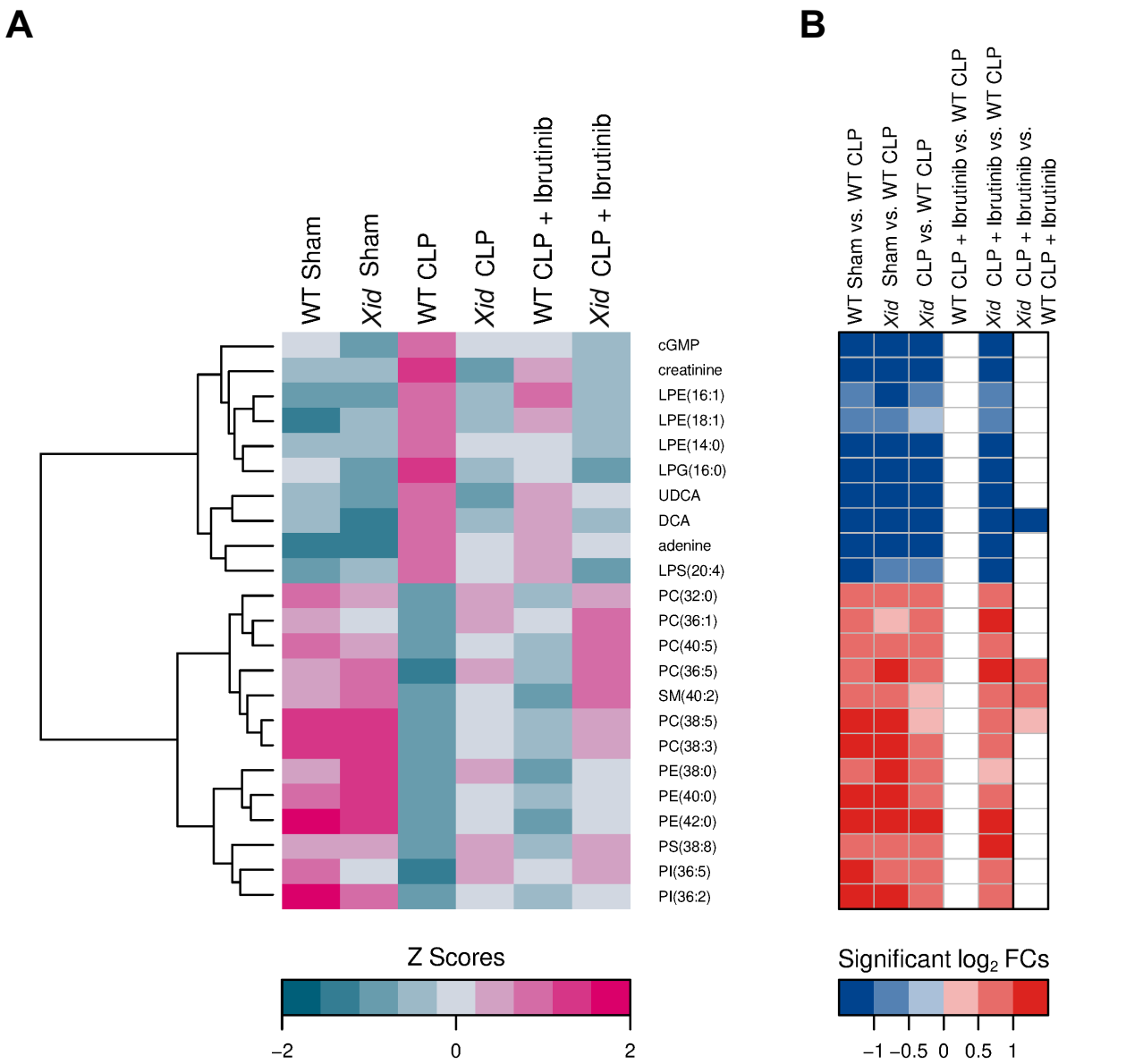

Figure S7. Heatmap of significant restored metabolites in two mice groups: *Xid*-CLP and *Xid* - CLP + Ibrutinib. (A) Hierarchical clustered z score heatmaps showed significantly changed metabolites. **(B)** log2 fold change heatmaps showed their significant log2 fold changes for selected groupwise comparisons The heatmap shows metabolites which, compared to the WT-CLP group (n = 10), restored in the groups *Xid*-CLP (n = 10) and *Xid* CLP + Ibrutinib (n = 6), but not in the WT-CLP + Ibrutinib (n = 8) and) to the level of the two sham groups (WT Sham (n = 5), *Xid* Sham (n = 5)). Each column in a z score heatmap represented the mean value of all animals in a group, each column in a log2 fold change heatmap represented a groupwise comparison and each row defined an analyte. Analytes were hierarchically clustered using Ward's minimum variance method and an euclidian distance between log2 fold changes. Dendrograms provide information about distances between clusters. cGMP: cyclic guanine monophosphate, DCA: deoxycholic acid, LPE: lysophosphatidylethanolamine, LPG: lysophosphatidylglycerol, LPS: lysophosphatidylserine, PC: phosphatidylcholine, PE: phosphatidylethanolamine, PI: phosphatidylinositol, PS: phosphatidylserine, SM: sphingomyelin, UDCA: ursodeoxycholic acid.

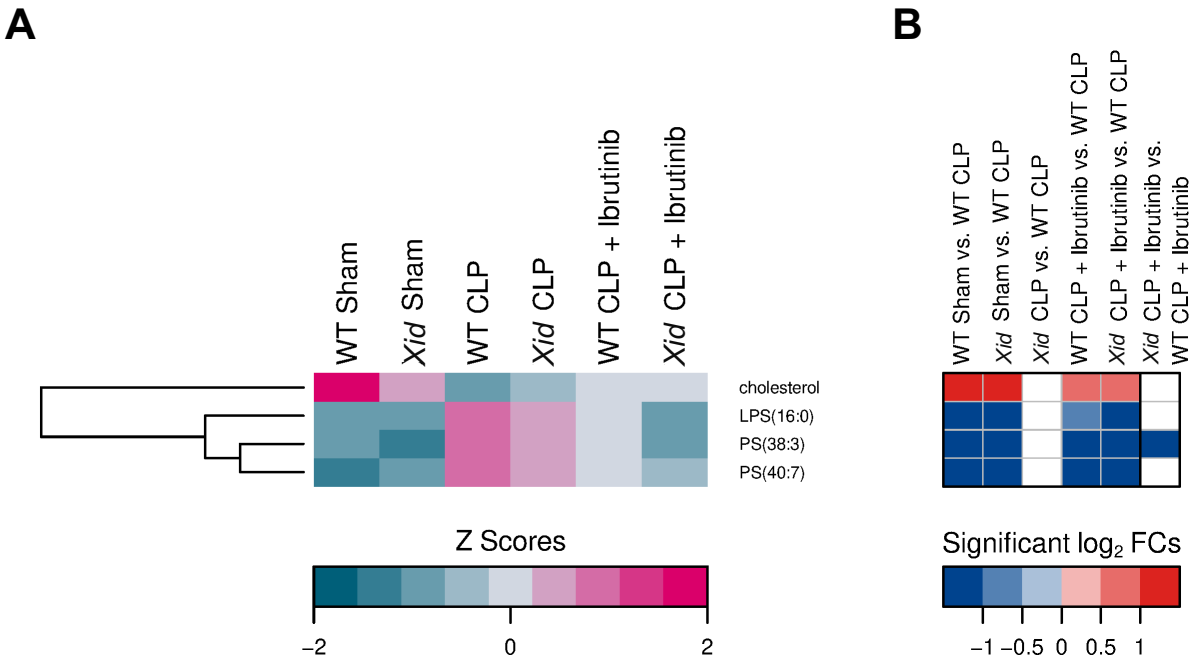

Figure S8. Heatmap of significant restored metabolites in two mice groups: WT CLP + Ibrutinib and *Xid* CLP + Ibrutinib. (A) Hierarchical clustered z score heatmaps showed significantly changed metabolites. **(B)** log2 fold change heatmaps showed their significant log2 fold changes for selected groupwise comparisons. The heatmap shows metabolites which, compared to the WT-CLP group (n = 10), restored in the groups WT-CLP + Ibrutinib (n = 8) and *Xid*-CLP + Ibrutinib (n = 6), but not in the *Xid*-CLP (n = 10) to the level of the two sham groups (WT Sham (n = 5), *Xid* Sham (n = 5)). Each column in a z score heatmap represented the mean value of all animals in a group, each column in a log2 fold change heatmap represented a groupwise comparison and each row defined an analyte. Analytes were hierarchically clustered using Ward's minimum variance method and an euclidian distance between log2 fold changes. Dendrograms provide information about distances between clusters. LPS: lysophosphatidylserine, PS: phosphatidylserine.

Supplementary tables

Table S1. UHPLC program. Solvent A consisted of 0.1% formic acid in water, solvent B consisted of 0.1% formic acid in acetonitrile, solvent C consisted of methanol and solvent D consisted of 2-propanol. The column oven temperature was set to 50 °C.

time [min]	flow [mL/min]	solvent A concentration [%]	solvent B concentration [%]	solvent C concentration [%]	solvent D concentration [%]	solvent B and C curve*
primary metabolites						
0.01	0.25	100				
2.00	0.25	100				
5.00	0.25	75				
11.00	0.25	65				
15.00	0.25	5				
20.00	0.25	5				
20.01	0.25	100				
25.00	stop					
lipid mediators						
0	0.2	90	10			
10.0	0.2	75	25			
20.0	0.2	65	35			
40.0	0.2	25	75			
40.2	0.2	5	95			
50.0	0.2	5	90			
50.2	0.2	90	10			
59.0	Stop					
phospholipids						
0.0	0.15	80	10		10	
2.0	0.15	80	10		10	

4.0	0.15	60	20	20	-3
50.0	0.15	7.6	46.2	46.2	
52.0	0.15	0	50	50	
70.0	0.15	0	50	50	
70.2	0.15	80	10	10	
80.0	stop				

sphingosine-1-phosphate and sphingosine

0	0.4	90	10
0.01	0.4	0	100
3.00	0.4	0	100
5.00	0.8	0	100
7.00	0.8	0	100
7.01	0.8	90	10
7.80	0.8	90	10
8.30	0.3	90	10
9.50	0.3	90	10
9.51	Stop		

*sets the gradient curve of the solvent (-10 to 10)

Table S2. Mass spectrometer (LCMS 8050) settings.

source conditions	parameters
nebulizing gas flow rate	3.0 L/min
heating gas flow rate	10.0 L/min
drying gas flow rate	10.0 L/min
collision-induced dissociation gas pressure	230 kPa
interface temperature	300 °C
desolvation line temperature	250 °C
block heater temperature	400 °C
ionization mode	electrospray ionisation (ESI)

Table S3: Mass transitions for identified significantly changed primary metabolites. The target ion shows the multiple reaction monitoring (MRM) transitions, the ionization polarity (IP) shows the ionization mode of the electrospray ionization (ESI) source and the internal standard (IS) column assigns the number of the internal standard to the compounds with which they were evaluated. The internal standard is marked in bold letters. Injection volume of 10 µl sample.

no.	compound	target ion	IP	IS
1	4-hydroxyproline	132.10>86.05	+	1
2	adenine	136.00>119.05	+	1
3	adenosine monophosphate	348.00>136.05	+	1
4	adenylsuccinic acid	464.10>252.10	+	1
5	alanine	89.90>89,90	+	1
6	arginine	175.10>70.10	+	1
7	argininosuccinic acid	291.00>70.10	+	1
8	asparagine	133.10>87.15	+	1
9	bilirubin	583.30>285.25	-	1
10	carnitine	162.10>103.05	+	1
11	carnosine	227.10>110.05	+	1
12	choline†	104.10>60.05	+	1
13	cholesterol	369.40>161.30	+	1
14	citrulline	176.10>70.05	+	1
15	creatine	132.10>44.05	+	1
16	creatinine	114.10>44.05	+	1
17	cystathionine	223.00>88.05	+	1
18	cystine	241.00>151.95	+	1
19	cytidine	244.10>112.05	+	1
20	cytidine 3',5'-cyclic monophosphate (cAMP)	306.00>112.10	+	1
21	cytidine monophosphate	324.00>112.05	+	1
22	cytosine	112.00>95.10	+	1

23	dihydroxyphenylalanine (DOPA)	198.10>152.10	+	1
24	dimethylarginine (symmetric/asymmetric)	203.10>70.15	+	1
25	dimethylglycine	104.10>58.05	+	1
26	flavin adenine dinucleotide	786.15>136.10	+	1
27	flavin mononucleotide	455.00>97.00	-	1
28	glutamic acid	147.90>84.10	+	1
29	glutamine	147.10>84.15	+	1
30	glutathione	308.00>179.10	+	1
31	guanosine 3',5'-cyclic monophosphate (cGMP)	346.00>152.05	+	1
32	guanosine monophosphate	364.00>152.05	+	1
33	histamine	112.10>95.05	+	1
34	histidine	155.90>110.10	+	1
35	isoleucine	132.10>69.15	+	1
36	kynurenine	209.10>192.05	+	1
37	leucine	132.10>30.05	+	1
38	lysine	147.10>84.10	+	1
39	niacinamide	123.10>80.05	+	1
40	nicotinic acid	124.05>80.05	+	1
41	ophthalmic acid	290.10>58.10	+	1
42	ornithine	133.10>70.10	+	1
43	phenylalanine	166.10>120.10	+	1
44	proline	116,10>70,15	+	1
45	oxidized glutathione	611.10>306.00	-	1
46	s-adenosylmethionine	399.10>250.05	+	1
47	serotonin	177.10>160.10	+	1
48	threonine	120.10>74.15	+	1

49	thymidine	243.10>127.10	+	1
50	thymidine monophosphate	322.90>81.10	+	1
51	tyrosine	182.10>136.10	+	1
52	uracil	113.00>70.00	+	1
53	uric acid	167.10>123.95	-	1
54	uridine	245.00>113.05	+	1
55	valine	118.10>72.15	+	1
56	**2-morpholinoethanesulfonic acid (IS)**	**194.00>80.15**	**-**	**1**

†illustrated in heatmaps of phospholipids

Table S4: Mass transitions for identified significantly changed phospholipids. The target ion shows the multiple reaction monitoring (MRM) transitions, the ionization polarity (IP) shows the ionization mode of the ESI source and the internal standard (IS) column assigns the number of the internal standard to the lipid species with which they were evaluated. The internal standard is marked in bold letters. (LPC: lysophosphatidylcholine, PC: phosphatidylcholine, LPE: lysophosphatidylethanolamine, PE: phosphatidylethanolamine, LPG: lysophosphatidylglycerol, LPI: lysophosphatidylinositol, PI: phosphatidylinsitol, LPS: lysophosphatidylserine, PS: phosphatidylserine, SM: sphingomyelin)

no.	lipid species	target ion	IP	IS
1	LPC(16:1)	494.3>184.10	+	1
2	LPC(18:1)*	522.4>184.10	+	1
3	LPC(18:3)	518.3>184.10	+	1
4	LPC(20:0)	552.4>184.10	+	1
5	LPC(20:1)	550.4>184.10	+	1
6	LPC(20:2)	548.4>184.10	+	1
7	LPC(20:3)	546.4>184.10	+	1
8	LPC(20:4)*	544.4>184.10	+	1
9	LPC(20:5)	542.3>184.10	+	1
10	LPC(22:0)	580.5>184.10	+	1
11	LPC(22:1)	578.4>184.10	+	1
12	LPC(22:6)*	568.4>184.10	+	1
13	PC(30:0)	706.6>184.10	+	1
14	PC(30:1)*	704.5>184.10	+	1
15	PC(30:2)*	702.5>184.10	+	1
16	PC(32:0)*	734.6>184.10	+	1
17	PC(32:1)*	732.6>184.10	+	1
18	PC(32:2)	730.6>184.10	+	1
19	PC(34:3)*	756.6>184.10	+	1
20	PC(36:0)	790.7>184.10	+	1
21	PC(36:1)*	788.6>184.10	+	1

22	PC(36:3)*	784.6>184.10	+	1
23	PC(36:5)*	780.6>184.10	+	1
24	PC(38:1)	816.7>184.10	+	1
25	PC(38:2)*	814.7>184.10	+	1
26	PC(38:3)*	812.6>184.10	+	1
27	PC(38:5)*	808.6>184.10	+	1
28	PC(38:7)*	804.6>184.10	+	1
29	PC(38:8)	802.6>184.10	+	1
30	PC(40:0)	846.7>184.10	+	1
31	PC(40:1)	844.7>184.10	+	1
32	PC(40:2)	842.7>184.10	+	1
33	PC(40:3)	840.7>184.10	+	1
34	PC(40:4)	838.7>184.10	+	1
35	PC(40:5)*	836.6>184.10	+	1
36	PC(40:7)*	832.6>184.10	+	1
37	PC(40:8)	830.6>184.10	+	1
38	PC(42:0)	874.8>184.10	+	1
39	PC(42:1)	872.7>184.10	+	1
40	PC(42:2)	870.7>184.10	+	1
41	PC(42:3)	868.7>184.10	+	1
42	PC(42:4)	866.7>184.10	+	1
43	PC(42:5)	864.7>184.10	+	1
44	PC(42:6)	862.7>184.10	+	1
45	PC(42:7)	860.6>184.10	+	1
46	PC(42:8)	858.6>184.10	+	1
47	PC(44:1)	900.8>184.10	+	1

48	PC(44:6)	890.7>184.10	+	1
49	PC(44:7)	888.7>184.10	+	1
50	LPE(14:0)	426.3>285.24	+	1
51	LPE(14:1)	424.3>283.23	+	1
52	LPE(16:0)	454.3>313.27	+	1
53	LPE(16:1)	452.3>311.26	+	1
54	LPE(18:0)	482.3>341.30	+	1
55	LPE(18:1)	480.3>339.29	+	1
56	LPE(18:2)	478.3>337.27	+	1
57	LPE(18:3)	476.3>335.26	+	1
58	LPE(20:0)	510.4>369.34	+	1
59	LPE(20:2)	506.3>365.30	+	1
60	LPE(20:3)	504.3>363.29	+	1
61	LPE(20:4)	502.3>361.27	+	1
62	LPE(20:5)	500.3>359.26	+	1
63	LPE(22:0)	538.4>397.37	+	1
64	LPE(22:1)	536.4>395.35	+	1
65	LPE(22:6)	526.3>385.27	+	1
66	PE(32:0)	692.5>551.50	+	1
67	PE(32:1)	690.5>549.49	+	1
68	PE(32:2)	688.5>547.47	+	1
69	PE(34:1)	718.6>577.52	+	1
70	PE(34:2)	716.5>575.50	+	1
71	PE(34:3)	714.5>573.49	+	1
72	PE(36:1)	746.6>605.55	+	1
73	PE(36:2)	744.6>603.53	+	1

74	PE(36:3)	742.6>601.52	+	1
75	PE(36:4)	740.5>599.50	+	1
76	PE(36:5)	738.5>597.49	+	1
77	PE(38:0)	776.6>635.60	+	1
78	PE(38:1)	774.6>633.58	+	1
79	PE(38:2)	772.6>631.57	+	1
80	PE(38:3)	770.6>629.55	+	1
81	PE(38:4)	768.6>627.53	+	1
82	PE(38:5)*	766.6>625.52	+	1
83	PE(38:7)	762.5>621.49	+	1
84	PE(40:0)	804.7>663.63	+	1
85	PE(40:4)	796.6>655.57	+	1
86	PE(40:5)	794.6>653.55	+	1
87	PE(40:6)	792.6>651.53	+	1
88	PE(40:7)	790.6>649.52	+	1
89	PE(40:8)	788.5>647.50	+	1
90	PE(42:0)	832.7>691.66	+	1
91	PE(42:1)	830.7>689.64	+	1
92	PE(44:0)	860.7>719.69	+	1
93	LPG(14:1)	455.3>283.14	+	1
94	LPG(16:0)	485.3>313.19	+	1
95	LPG(16:1)	483.3>311.17	+	1
96	LPG(18:1)	511.3>339.20	+	1
97	LPG(18:2)	509.3>337.19	+	1
98	LPI(16:0)	571.3>241.01	-	1
99	LPI(18:0)	599.3>241.01	-	1

100	LPI(18:1)	597.3>241.01	-	1
101	LPI(18:2)	595.3>241.01	-	1
102	LPI(20:4)	619.3>241.01	-	1
103	LPI(22:6)	643.3>241.01	-	1
104	PI(34:1)	835.6>241.01	-	1
105	PI(34:2)	833.5>241.01	-	1
106	PI(36:1)	863.6>241.01	-	1
107	PI(36:2)	861.6>241.01	-	1
108	PI(36:3)	859.6>241.01	-	1
109	PI(36:4)	857.5>241.01	-	1
110	PI(36:5)	855.5>241.01	-	1
111	PI(38:4)	885.6>241.01	-	1
112	PI(38:5)	883.6>241.01	-	1
113	PI(38:6)	881.5>241.01	-	1
114	PI(40:6)	909.6>241.01	-	1
115	LPS(16:0)	498.3>313.26	+	1
116	LPS(18:0)	526.3>341.29	+	1
117	LPS(18:1)	524.3>339.28	+	1
118	LPS(18:2)	522.3>337.26	+	1
119	LPS(20:4)	546.3>361.26	+	1
120	LPS(22:6)	570.3>385.26	+	1
121	PS(34:1)	762.6>577.51	+	1
122	PS(36:1)	790.6>605.54	+	1
123	PS(36:2)	788.6>603.52	+	1
124	PS(36:4)	784.5>599.49	+	1
125	PS(36:5)	782.5>597.48	+	1

126	PS(36:6)	780.5>595.46	+	1
127	PS(38:3)	814.6>629.54	+	1
128	PS(38:4)	812.6>627.52	+	1
129	PS(38:6)	808.5>623.49	+	1
130	PS(38:8)	804.5>619.46	+	1
131	PS(40:4)	840.6>655.56	+	1
132	PS(40:5)	838.6>653.54	+	1
133	PS(40:6)	836.6>651.52	+	1
134	PS(40:7)	834.6>649.51	+	1
135	SM(32:1)	675.6>184.10	+	1
136	SM(32:2)	673.6>184.10	+	1
137	SM(34:2)	701.6>184.10	+	1
138	SM(36:1)	731.6>184.10	+	1
139	SM(36:2)	729.6>184.10	+	1
140	SM(36:3)	727.6>184.10	+	1
141	SM(36:4)	725.6>184.10	+	1
142	SM(38:2)*	757.6>184.10	+	1
143	SM(38:6)	749.6>184.10	+	1
144	SM(40:2)*	785.7>184.10	+	1
145	**sphingosine-1-phosphate (17:0) IS**	**366.3>250.4**	**+**	**1**

*0.5 µl sample injection volume

Table S5: Mass transitions for identified significantly changed lipid mediators. The target ion shows the multiple reaction monitoring (MRM) transitions, the ionization polarity (IP) shows the ionization mode of the ESI source and the internal standard (IS) column assigns the number of the internal standard to the lipid mediators with which they were evaluated. The internal standard is marked in bold letters.

no.	compound		target ion	IP	IS
1	9,10-DiHOME	9,10-dihydroxy-octadecenoic acid	313,2>201,2	-	1
2	14-HDoHE	14-hydroxy-docosahexaenoic acid	343,2>205,2	-	1
3	19-HETE	19-hydroxyeicosatetraenoic acid	319,2>275,2	-	1
4	AA	arachidonic acid	303,2>303,2	-	1
5	cholic acid†		407.25>407.25	-	1
6	DCA†	deoxycholic acid	391.30>391.30	-	1
7	DHA	docosahexaenoic acid	327,2>283,2	-	1
8	EPA	eicosapentaenoic acid	301,2>257,2	-	1
9	GLCA†	glycolithocholic acid	432.30>432.30	-	1
10	Lyso-PAF	lyso-platelet activating factor	482,3>184,1	-	1
11	OEA	oleoylethanolamine	326,2>62,1	+	1
12	TCDCA†	taurochenodeoxycholic acid	498.40>498.40	-	1
13	TDCA†	taurodeoxycholic acid	498.40>498.40	-	1
14	UDCA†	ursodeoxycholic acid	391.30>391.30	-	1
15	**S1P (17:0) IS**	**sphingosine-1-phosphate (17:0) IS**	**366.3>250.4**	+	**1**

†illustrated in heatmap of primary metabolites

Table 6: Mass transitions for sphingosine-1-phosphate and sphingosine. The target ion shows the multiple reaction monitoring (MRM) transitions, the ionization polarity (IP) shows the ionization mode of the ESI source and the internal standard (IS) column assigns the number of the internal standard to the compounds with which they were evaluated. The internal standard is marked in bold letters.

no.	compound	target ion	IP	IS
1	sphingosine-1-phosphate†	380.3>264.4	+	1
2	sphingosine†	300.4>282.4	+	1
3	**sphingosine-1-phosphate (17:0) IS**	**366.3>250.4**	**+**	**1**

†illustrated in heatmap of phospholipids II

Supplementary Table 7. Average concentration of cytokines in serum. Mice underwent sham or CLP surgery, 24 h later 31 cytokines and chemokines were assessed in serum. Data are expressed as mean ± SEM (pg/ml). The following groups were studied WT sham (n = 5), *Xid* sham (n = 5), WT-CLP (n = 10), *Xid*-CLP (n = 10), WT-CLP + ibrutinib (n = 8), *Xid*-CLP + ibrutinib (n = 6).

	WT Sham		***Xid* Sham**		**WT CLP**		***Xid* CLP**		**WT CLP + ibrutinib**		***Xid* CLP + ibrutinib**	
	Mean	SEM +/-	Mean	SEM +/-	Mean	SEM +/-	Mean	SEM +/-	Mean	SEM +/-	Mean	SEM +/-
BCA-1/CXCL13	7034.2	3097.9	8937.8	2330.0	83810.3	4310.6	77435.3	2269.3	85285.5	3220.6	80840.9	1375.5
CTACK/CCL27	1872.3	202.1	2327.4	398.1	3886.4	339.4	8395.2	1781.0	7661.8	1191.3	7369.2	1032.9
ENA-78/CXCL5	1980.0	772.6	2831.5	987.5	45770.7	5248.7	8462.4	969.7	11727.6	2524.8	7210.7	982.8
Eotaxin/CCL11	420.6	151.2	733.3	171.2	6869.6	356.5	1952.5	224.5	2690.1	465.2	1907.8	179.3
Eotaxin-2/CCL24	13102.7	4999.2	18708.2	3000.5	56736.3	5714.4	25735.7	2079.7	11983.1	1876.6	29652.0	3562.5
Fractalkine/CXCL1	264.5	9.1	279.7	17.5	1181.9	109.7	322.8	12.2	457.7	47.5	352.9	20.4
GM-CSF	5.4	0.8	5.4	0.7	346.2	58.6	7.5	1.1	14.7	3.2	7.7	0.7
I-309/CCL1	45.6	4.9	58.4	14.0	198.7	66.5	799.7	190.5	80.1	15.6	11691.8	9593.7
IFN-γ	133.8	11.1	155.5	17.5	134.0	16.2	102.3	15.1	98.1	28.8	191.6	14.4
IL-1β	680.0	57.0	706.3	72.6	1536.3	184.7	674.6	31.4	611.0	43.8	768.9	28.0
IL-2	11.7	2.6	15.9	4.0	38.3	7.8	102.6	25.8	72.8	15.4	57.4	18.7
IL-6	45.5	4.8	52.6	6.7	524272.8	43243.2	6380.9	1557.2	29367.0	18095.0	4296.7	1827.7
IL-4	74.7	3.6	87.5	8.0	65.2	3.9	76.0	8.0	52.3	9.2	92.0	3.5
IL-10	1296.5	84.4	1677.4	159.6	23882.5	2465.0	2077.0	370.9	3485.3	947.8	2252.3	362.6
IL-16	978.4	68.9	1048.3	87.4	2836.1	207.4	1313.4	86.9	1814.6	200.3	1462.5	95.6
IP-10/CXClL10	4561.3	205.3	4994.1	536.0	4837.9	327.2	4547.3	583.3	4036.2	420.8	5182.1	157.5
I-TAC/CXCL11	4666.7	272.0	5570.1	490.2	3217.0	291.5	3372.9	340.1	2991.7	826.7	5569.5	376.0
KC/CXCL1	298.0	24.0	337.9	24.5	158693.9	35967.2	9014.0	1570.5	16952.6	6344.1	8912.3	2432.5
MCP-1/CCL2	515.8	36.3	601.9	59.7	262035.2	117148.0	9660.5	3217.7	10558.8	3887.3	3100.1	531.8
MCP-5/CCL12	24.0	4.9	31.6	4.5	5348.5	785.1	935.7	129.2	1020.6	157.1	758.3	70.1
MDC/CCL22	190.9	41.0	210.3	35.3	1869.7	235.7	494.0	48.3	515.9	36.1	717.8	69.6
MIP-1α/CCL3	27.5	2.1	34.0	3.7	4994.4	1664.0	175.4	56.9	81.7	24.5	56.1	2.2
MIP1-β/CCL4	123.9	6.9	141.1	12.9	51791.1	19413.9	1445.3	372.8	2859.4	1022.9	509.2	68.5
MIP-3α/CCL20	38.8	3.4	41.7	4.4	893.8	117.3	691.2	157.2	549.9	176.4	1134.8	163.6
MIP-3β/CCL19	2285.8	104.5	2520.6	204.6	3622.2	350.3	3830.6	351.0	2933.2	242.3	4925.1	465.9
Rantes/CCL5	28.8	5.4	33.4	5.9	2647.5	421.4	80.0	10.3	487.9	148.7	110.0	24.3
SCYB16/CXCL16	601.1	133.4	748.4	91.0	4588.5	467.1	2250.7	317.4	2440.4	447.1	1851.1	266.6
SDF-1α/CXCL12	929.5	197.3	1263.0	218.9	447.7	63.0	1612.0	177.7	1113.3	341.6	2304.9	389.7
TARC/CCL17	115.6	16.7	146.8	21.6	3293.6	376.2	2269.2	441.2	755.4	114.8	5268.3	1862.4
TNF-α	311.2	16.7	310.6	28.0	471.7	42.9	205.1	16.5	208.5	38.7	330.8	27.1